On The Reductions of Airfoil Broadband Noise through Sinusoidal Trailing-Edge Serrations

Sushil Kumar Singh [1], Mohit Garg [2], S. Narayanan [3],*,
Lorna Ayton [4] , Paruchuri Chaitanya [5]

Abstract

The present study investigates the efficacy of sinusoidal trailing edge (TE) serrations as a passive means for the reductions of airfoil broadband noise, theoretically and experimentally. Comprehensive parametric studies are conducted to determine the effect of serration amplitudes and wavelengths on the noise reduction performance of a NACA airfoil. Initially, the present paper shows the use of the Trailing-Edge Noise Model (TNO) for the accurate predictions of the surface pressure spectrum near the TE and hence the far-field noise using the Wiener-Hopf method. The predicted spectra and the noise reduction levels showed good agreement with the measurements for a wide range of frequencies. The present study reveals that the local maxima of the overall noise reductions occur when the transverse turbulence integral length scale is either 1.2 or 0.2 times the serration wavelength, which corresponds to $\lambda/\Lambda_t = 0.833$ or 5, where λ and Λ_t are the serration wavelength and integral length scale. One of the key findings of the paper is that the serration wavelength at which the highest noise reductions occur when the acoustic emissions vary inversely with the modified Strouhal number S_{thm} (i.e., $w_{sste}(\omega)/w_{bl}(\omega) \propto 1/S_{thm}$) for narrow (i.e., small wavelengths) and wider serrations (i.e., large wavelengths), where w_{sste} and w_{bl} are the acoustic emissions radiated from the serrated and baseline airfoils. Further, the TE serrations are also observed to reduce leading-edge (LE) noise along with the self-noise, which indicates the efficacy of TE serrations in reducing the total far-field noise.

Keywords: Airfoil, turbulent flows, trailing edge, sinusoidal serrations, broadband noise

---

[1]Research Scholar, Department of Mechanical Engineering, IIT (ISM), Dhanbad-826004, India. Email: sushilkr243@gmail.com.

[2]Undergraduate student, Department of Mechanical Engineering, IIT (ISM), Dhanbad-826004, India. Email: garg.26.mohit@gmail.com,

[3]Associate Professor, Department of Mechanical Engineering, IIT (ISM), Dhanbad – 826004, India*Corresponding author, Email: narayan@iitism.ac.in/snarayan.1979@gmail.com (S. Narayanan)

[4]Researcher, Department of Applied Mathematics and Theoretical Physics, University of Cambridge, Cambridge CB3 0WA, UK Email: lja30@cam.ac.uk

[5]Lecturer, Faculty of Engineering and the Environment, University of Southampton, Southampton SO17 1BJ, UK. Email: mail2pcc@gmail.com

1. Introduction

The acoustic emissions from various lifting surfaces, such as airfoils, turbine blades, fan blades, etc. are of primary concern in several strategically important sectors in the country, including environment, energy, and transport. It is an important obstacle for the expansion of airport traffic and the proper deployment of on-shore wind farms. This paper aims to overcome this problem by developing novel airfoil trailing edge (TE) designs that are effective in reducing overall far-field noise over a broad range of operating conditions. The acoustic radiations in aircraft can arise from different sources such as airfoil-turbulence noise (ATI), airframe noise, pylon noise, landing gear noise, etc. Out of these, fan broadband noise i.e., ATI is the primary noise source from the civil aircraft except during the landing. The reductions of airfoil-turbulence noise are imperative for the development of new airports as well as the expansion of the existing airports since they create huge noise pollutions to the surrounding environments. Also, the noise generated creates a lot of health-hazardous like sleep disturbance, hearing impairment, etc., to those who are living close to the airports. Earlier studies revealed that airfoil broadband noise is considered as the dominant source from commercial aircraft and hence immediate attention is required for the mitigation of the airfoil broadband noise. Because of the growing aircraft industry in the early 1990s and the development of wind farms later, researchers started addressing the airfoil trailing edge noise problem using various passive treatments such as serrations, brushes, and porous trailing edges. Although several works of literature are available for the control of airfoil broadband noise through various serration geometries, the novel idea of providing sinusoidal i.e., wavy trailing edge (TE) serrations for reducing airfoil broadband noise are scarce. Therefore, this paper provides a detailed experimental investigation into the use of sinusoidal trailing edge serrations as a passive means for minimizing airfoil broadband noise. For this, a systematic parametric study is performed for different serration amplitudes $2h$ and wavelengths λ to determine the key serration parameters i.e., λ and h of the foil which provide the best noise reductions over a wide range of frequencies. Some of the pertinent literature on the airfoil trailing edge noise are given below:

Amiet [1–3] developed a theoretical method for predicting the far-field acoustic radiations from an airfoil placed in a turbulent stream and later he extended this theory to predict the trailing edge noise. For predicting the trailing edge noise, he used the surface pressure spectrum upstream of the trailing edge as a suitable input. In this study, the noise is considered as produced by the surface dipoles close to the trailing edge. He observed that the trailing edge noise from the airfoil is typically very small as compared to those generated by the oncoming turbulence levels of 1%.

Azarpeyvand et al.[4] analytically and numerically, investigated the trailing edge noise reduction of a semi-infinite flat plate using periodic trailing edge serrations. They developed analytical expressions to predict far-field acoustic spectra for various serrations such as sawtooth, sinusoidal, slitted, slitted-sawtooth, and sawtooth-sinusoidal. They noticed that the far-field acoustic radiations could be substantially reduced by applying complex periodic serrations at the trailing edge of the foil. Further, they showed that the slitted sawtooth serration is the best serration geometry for the reduction of trailing edge noise from low to mid-frequency ranges.

Bachmann et al.[5] systematically, compared the acoustic radiation characteristics of a barn owl's feathers with a pigeon one and accentuated the specific characteristics of the owl's feathers on macroscopic/microscopic levels, which are liable for the generation of sound. They found that the owl generates slow noise as compared to the pigeon due to the existence of tubercles (i.e., serrations) at the wing's leading edge and fringes at the edges. They proposed that the mechanisms responsible for the noiseless flight of the owl could be utilized for aerodynamic benefits, which might result in the development of new wings for modern aircraft.

Brooks et al.[6] developed a semi-empirical prediction method for the self-noise generated from an airfoil placed in a smooth flow. Five self-noise mechanisms such as (1) Turbulent boundary layer trailing edge noise, (2) Laminar boundary layer vortex shedding, (3) Separation stall noise, (4) Trailing edge bluntness - vortex shedding noise, and (5) Tip vortex noise, due to specific boundary layer phenomena were identified and modeled. The predictions were observed to match well with the measurements made on seven NACA0012 airfoils of various sizes in a wind tunnel up to a Mach number of 0.21 for the range of angles of attack from 0^o to 25.2^o. Also, they noticed that the predictions showed good agreement with the published data for the three self-noise studies made on various airfoil geometries up to a Mach number of 0.5. Further, they showed that the prediction method matched very well with the rotor broadband noise measured in a large anechoic wind tunnel.

Gruber [7] experimentally, investigated the use of saw-tooth serrations as a passive means for reducing airfoil broadband noise. They studied the effect of various serration parameters namely, (i) serration height and (ii) serration wavelength on the noise reduction performance of the foil for various jet velocities and angles of attack. They showed that sharper serrations provide superior far-field noise reductions. They observed noise reductions of up to $5\,dB$ up to a certain critical frequency, beyond which the noise level increases. They revealed that the noise reduction arises due to the attenuation of the interaction between the incident and scattered pressures, which results in the decrease of the phase speed along the serrated edges as compared with the straight ones.

Dassen et al.[8] experimentally, investigated the effect of trailing edge serrations on airfoils and flat plates for the reductions of airfoil self-noise. They observed that the serrated plates provided noise reductions of up to 10 dB from 1 to 6 kHz, while serrated airfoils showed reductions from up to $8\ dB$. They noticed that the misalignment of the teeth by 10^o relative to flow direction provided noise reductions less than $2\ dB$, while an increase of the radiated noise is observed for 15^o.

Oerlemans et al.[9] characterized the acoustic sources of the rough blade, clean blade tripped blade, and untreated blade to check the dominancy of the trailing edge noise for the range of jet speeds from 6 to 10 ms^{-1}, using a large horizontal microphone array of about $58\ m$. They observed that the blades generate higher noise radiations to the ground during their downward movement than the rotor hub. Also, they noticed that the blade noise is mainly generated in the outer section of the blades rather than the tip. Further, they observed that the tripped blade generates higher noise radiations as compared to the other cases mentioned above.

Moreau and Doolan [10] experimentally, studied the noise reduction performance of the saw-tooth trailing edge serrations of a flat plate airfoil for the range of chord-wise Reynolds numbers from 1.6×10^5 to 4.2×10^5. They observed that the trailing edge serrations could provide noise reductions of up to 13 dB in the narrow band noise levels due to the attenuation of the trailing edge vortex shedding. Also, they revealed that the mechanism of noise reduction is due to the influence of the trailing edge serrations on the hydrodynamic field at the location of the source.

Dassen et al.[11] predicted the trailing-edge noise using the newly developed model and compared the predicted spectra with the measured one. They revealed that the noise generation induced by the suction side turbulence is predicted accurately while those produced by the pressure side turbulence are slightly over predicted.

Sivakumar [12] experimentally, investigated six different trailing edge (TE) serration geometries, namely, (i) three serrations with a single large triangular geometry at the TE, (ii) two serrations with varying orientation with respect to the airfoil, and (iii) straight-edged baseline plate, on the flow-induced noise of an airfoil for the range of chordwise Reynolds numbers from 1.8×10^5 to 5.7×10^5. They observed substantial noise reductions of up to 6 dB for the triangular serrations with included angles less than 45^o, which showed good agreement with Howe's prediction. Also, they observed the highest noise reductions for the frequencies above $5\ kHz$ where the TE noise dominates over the leading edge (LE).

Doolan and Moreau [13] reviewed the earlier experimental trailing edge noise studies and compares the measured noise data for the NACA0012 airfoil with the two numerical predictions. The literature review and comparison showed the (i) extent of the available data, (ii) scatter in the results, and (iii) cause of the scatter. They also suggested the requirements of new experimental and numerical studies for understanding the physics of sound generation in detail.

Chong et al. [14] experimentally, investigated the reductions self-noise by introducing non-flat plate saw-tooth serrations at the trailing edge of an airfoil. They observed that the non-flat plate type serrations provide significant reductions of the broadband self-noise as well as the elimination of the high-frequency noise observed with flat plate type serrations. Also, they noticed that the narrowband vortex shedding noise due to the bluntness at the root of the serration is less pronounced for wider serration angles. Further, they used non-flat plate type trailing edge serration with woven-wire mesh for the control of the narrowband vortex shedding noise.

Herr and Dobrzynski [15] experimentally, studied the aeroacoustic and aerodynamic effects of trailing edge brush devices in DLR's AWB for the range of Reynolds numbers from 2.1×10^6 to 7.9×10^6. They found that the trailing edge noise frequencies scales with Strouhal number based on a reference length and the radiation intensities follow a velocity to the fifth power law, for both the reference and the brush trailing edge geometries. Further, they found that the length of the brush edge is a key parameter for the reduction of the trailing edge noise. They observed that the presence of brush at the trailing edge results in the suppression of narrow band bluntness noise as well as the reduction of the broadband noise.

Zhou et. al. [16] experimentally and theoretically, studied the effects of the velvety structures on the TE noise as well as the boundary layer characteristics of a flat plate model. They found that the velvety coating modifies the boundary layer characteristics as well as the TE noise spectrum. They noticed that the velvety coating suppresses the vortex shedding phenomena. Also, they found that the presence of velvety coating can provide significant reductions of the high-frequency noise by reducing the wall-normal velocity gradient and turbulent intensities near the wall.

Sandberg et. al. [17] investigated the potential noise reduction mechanism of a NACA-0012 airfoil. They used an immersed boundary method, which was capable of representing arbitrary three-dimensional geometries, for direct noise computations of various configurations that were not previously feasible.

Avallone et. al. [18] experimentally, studied the mechanism of the TE noise convecting the turbulent boundary layer of the NACA0018 airfoil. They showed that the flow pattern is more complex at the near wake than at upstream of the serration which was characterized by counter-rotating stream-wise-oriented vortical structures due to root and tip of the serration. They, also found that the conventional assumption of frozen turbulence adopted in the analytical model may limit the correct prediction of the far-field noise in the presence of spanwise-varying trailing-edge geometries.

León et. al. [19] investigated the flow past a NACA 0018 airfoil model having the saw-tooth trailing Edge. They noticed that the presence of stream-wise vortices that originates from the TE is primarily influenced by the serration flap angle. They also noticed that the TE noise was reduced at lower frequencies but higher frequencies, the noise level increases.

Although several studies are available on different TE serrations such as slits, sawtooth, sawtooth with holes, slitted sawtooth Gruber [7] for the control of airfoil self-noise but detailed systematic parametric experimental study on the sinusoidal TE serrations for the control of overall noise is very limited in the literature. Further, the idea of sinusoidal LE serrations evolved from the biomimetics of barn owl wing, which is applied on the TE of the airfoil in the present study to reduce the overall broadband noise. It is expected that the sinusoidal serrations have smooth tips/roots and hence better mixing of the boundary at the root is possible, which reduces scattering as compared to sharper sawtooth serrations. Therefore, the present study aimed at understanding the effect of smooth sinusoidal TE serrations for the reductions of airfoil overall broadband noise. The literature mentioned above clearly reveals that the TE serrations are a potential device for minimizing airfoil broadband noise, however, the detailed systematic parametric experimental study of the sinusoidal TE serrations for the control of airfoil broadband noise is nearly limited. Therefore, the present study aimed at understanding the effect of sinusoidal TE serrations as a passive means for the reductions of total aerodynamic noise over a wide range of frequencies. For this, a total of 32 serrated airfoil geometries comprising all combinations of the sinusoidal TE serrations with wavelengths (λ/C_0) of $0.0333,\ 0.0667,\ 0.10,\ 0.1333,\ 0.2$ and amplitudes (h/C_0) of $0.0333,\ 0.0667,\ 0.10,\ 0.1333,$ and 0.1667 are systematically investigated to quantify the effect of different serration parameters on the airfoil noise reductions. The studies are performed for various jet speeds of $20,\ 30,\ and\ 40\ ms^{-1}$. The far-field acoustic radiations of different TE serrated airfoils are compared with baseline NACA65(12)10 airfoil i.e., un-serrated TE to determine the best serration parameters which provide the highest noise reductions over a wide range of frequencies. Further, the noise reduction performance of the sinusoidal TE serrated airfoils is quantified by finding the relation between the turbulence integral length scale and serration wavelengths, which provide maximum noise reductions.

2. Experimental set-up and procedure

2.1. Test models studied

A NACA65(12)10 airfoil [$150\,mm \times 310\,mm$] with a slot at the trailing edge (TE) was 3D printed using ABS (Acrylonitrile butadiene styrene) material to obtain a smooth surface. The height and depth of the slot are kept as 10mm and 15mm, respectively for mounting different serration inserts. The different serration inserts are made using the laser i.e., laser cut in a $2\,mm$ thick acrylic sheet. Far-field acoustic measurements are conducted for various TE serration parameters to quantify the effect of serration parameters on the noise reduction performance of the airfoil. Also, the introduction of serration inserts into the slot of the airfoil results in the formation of a small step near the trailing edge which may affect the flow dynamics. Therefore, speed tapes are provided over the step to obtain smooth flow when it passes through the junctions between the airfoil surface and the serration insert. Schematic of the sinusoidal serration showing various parameters, as well as a photograph of the 3D printed NACA65 (12)10 airfoil with TE serrations are shown in [Fig. 1]. In the present study, the serration geometries are limited to sinusoidal (i.e., wavy) profiles, since the effects of these profiles at the trailing edge of the airfoil were not systematically studied in detail for the reductions of airfoil broadband noise. The chord length of the TE serrated NACA65(12)10 airfoil with an amplitude h and wavelength λ is given in Eqn. (1) by Narayanan et al. [20] as follows:

$$C(y) = C_0 + h \sin(2\pi y/\lambda) \quad (1)$$

where C_0 is the mean chord and y is the span-wise distance.

2.2. Open-jet wind tunnel facility

An open-jet wind tunnel facility is placed inside an in-house built anechoic chamber with an overall working space of *2.6 m x 1.7 m x 2.20 m* (tip-to-tip) developed at IIT (ISM) Dhanbad. It is used for generating flow over airfoils. Sushil et al. [21] found that the lower cut-off frequency of the built anechoic chamber is *315 Hz* within $\pm 0.5\ dB$.

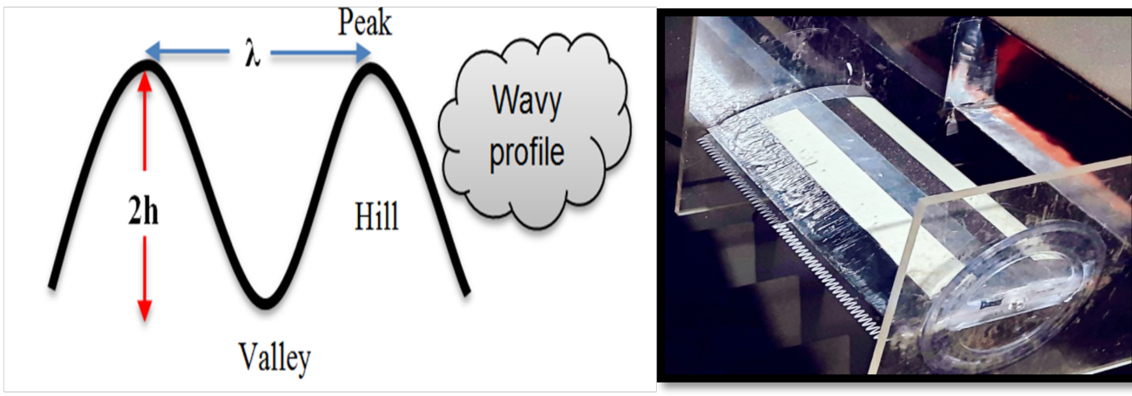

(a) **(b)**

Fig.1. (a) Schematic of the sinusoidal serration showing various parameters, (b) TE serrated airfoil, used in the present study

This indicates that the chamber is anechoic for the range of frequencies of interest (i.e. from 1 to 15 kHz) of the present study. The jet flow to the open jet tunnel is given by a centrifugal fan (Capacity: $10000\ m^3hr^{-1}$, Max RPM: *2936*) mounted on the slab driven by a *20 HP* motor. Anti-vibration pads are provided on the slab for damping the excessive vibrations caused due to shaking of the blades. A variable frequency drive (Make: CG Power, Model: VSU48-024-20CNB) is used to vary the speed of the motor. The air from the fan initially passes through a transition piece to a rectangular duct mounted on the wall and is then guided by a diffuser. Subsequently, the flow enters a settling chamber provided with a series of meshes/honeycomb sections to obtain a low noise and uniform flow. Ultimately, the flow passes through a rectangular nozzle having a contraction ratio of 8:1. The height/width of the nozzle exit is *0.15 / 0.30 m*, respectively. The schematic and photograph of the experimental facility are given in [Fig. 2] and [Fig. 3]. In this facility, the flow speed can be varied between $20\ to\ 50\ ms^{-1}$. The baseline and serrated airfoil test models are kept in the turbulent stream using two side plates to sustain two-dimensional flow, as shown in [Fig. 3b].

To maintain the quiet and uniform flow, wire meshes and honeycombs and are provided in the settling chamber. In the open jet wind tunnel, the jet deflection occurs and hence the geometric angle of attack and effective angle of attack will be different, which can be taken care of by correction in the angle of attack. In real aircraft, the jet deflection will not occur and hence the correction is not required. So, open jet wind tunnels are generally used for smaller angles of attack. With the aid of Kevlar extensions, open jet wind tunnels can be used for higher angles of attack. The present study is done for smaller angles of attack and hence Kevlar extensions are not required.

As pointed out by Brooks et al. [6], in the presence of an airfoil, the flow from the open-jet wind tunnel is deflected downwards. As this deviation does not occur in free air, it is important to correct for it to determine the effective angle of attack *(α)* in free air. In the present paper, all the experiments are conducted at *0°* geometric angle of attack since the effective angle of attack is same as the geometric one in the present study. Also, the far-field noise characteristics show similar behavior at low angles of attack. The correction of the geometrical angle of attack is reported by Gruber [7] in which he explained that the geometrical angle of attack α_g is corrected by considering the geometrical factor ζ to obtain the equivalent angle in free air α_e for an equivalent lift force. The geometrical angle of attack α_g of the test rig is defined as the angle between the flow and the chord line. The effective angle of attack $\alpha_e = \alpha_g/\zeta$, where, $\zeta = (1+2\sigma)^2 + \sqrt{12\sigma}$, and $\sigma = \frac{\pi^2}{48}\left(\frac{c}{H}\right)^2$ and c and H are the airfoil chord and the height of the jet, respectively.

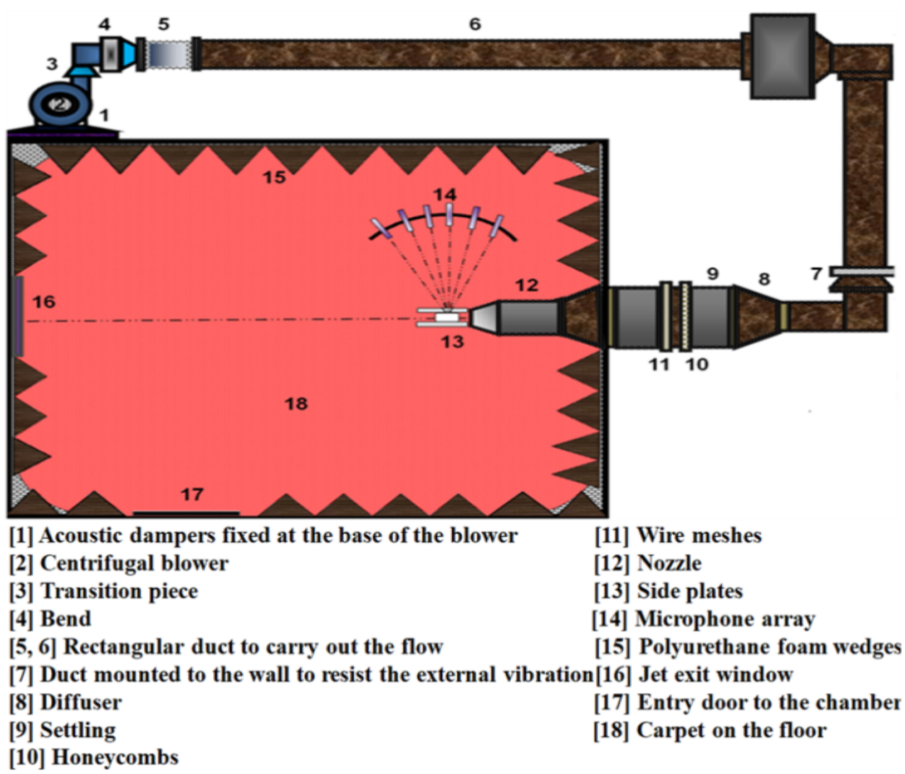

Fig.2. Schematic of the open jet wind tunnel setup placed inside an anechoic chamber

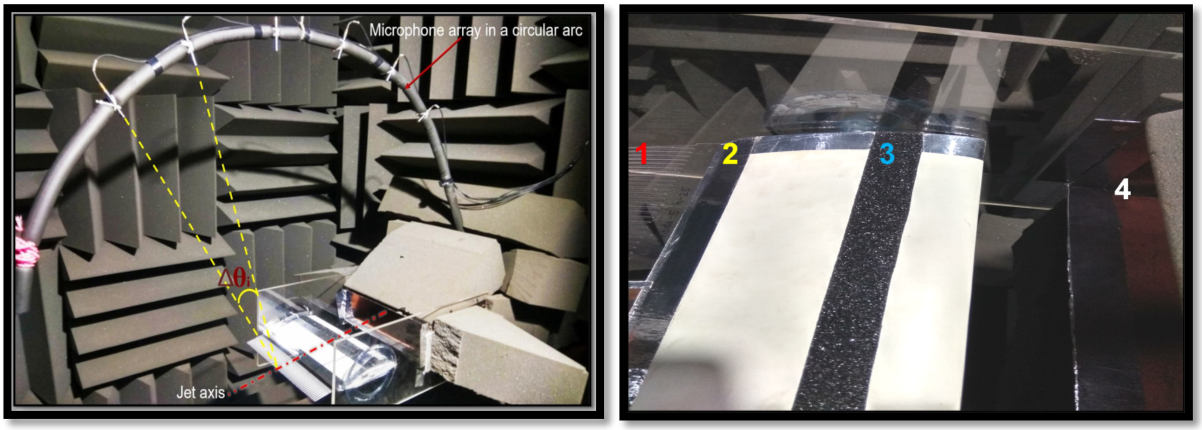

(a) **(b)**

[1]Wavy Serration
[2]Speed Tape
[3]Rough Band Tape
[4]Nozzle Exit

Fig.3. Photographs of (a) microphone array comprising of six free-field condenser microphones placed at an equidistant distance from the center of the airfoil inside an anechoic open jet wind tunnel facility, (b) TE serrated NACA airfoil placed in the turbulent stream.

2.3. Measurement and Instrumentation

Far-field noise measurements from the airfoils are made using an array of a six-quarter-inch free-field condenser microphone (Make: GRAS, Model no.:40PH 277551) having a sensitivity of $50\ mVPa^{-1}$ at $250\ Hz$. The radius of the microphone array is $0.65\ m$ from the trailing edge of the airfoil. These microphones are positioned between emission angles of 60^o *and* 135^o measured relative to the downstream jet axis. Noise measurements are carried for a $10\,s$ duration at a sampling frequency rate of $50\,kHz$. The data is transferred to a PC using NI 15 LABVIEW software through a four-channel simultaneous sampling data acquisition system (Make: NI, Model: channel Chassis- CDAQ 9174, Module: NI 9222 C Series). The recorded time-series data is divided into FFT blocks of 1024 data points each. The acoustic spectra obtained from each FFT block are averaged and the Hanning window is used to determine FFT. Acoustic data are recorded for the three mean jet velocities (U) of *20, 30, and 40* ms^{-1}. The jet velocity is measured using a digital manometer (Make: PCE, Model: HVAC-2). The sound power level is calculated by integrating the pressure spectra over the polar array of six microphones. Sound power level reductions are determined by subtracting sound power radiated by the serrated airfoil from the baseline straight edge profile as shown in Eq. (5). To prevent the presence of tonal noise component in the far-field, which generally arises due to Tollmien-Schlichting (T-S) instability waves convecting in the laminar boundary layer, the flow in the vicinity of the airfoil's leading edge is tripped using a rough tape on both the sides (i.e., suction and pressure) of the airfoil to obtain fully developed turbulence in the boundary layer. The acoustic radiation is expressed in terms of sound pressure level spectrum SPL, defined in Eq. (2)

$$\text{SPL}\ (f) = 20\log_{10} \left[\!\left[\frac{S_{pp}(f)}{p_{ref}} \right]\!\right] \tag{2}$$

where $S_{pp}(f)$ is the spectral density of the acoustic pressure and $p_{ref} = 20 \times 10^{-6}\ Pa$.

The spectral density of the acoustic power $S_w(f)$radiated between the emission angles [$60°$–$135°$], $w_{ref} = 10^{-12}\ W$, $\Delta\theta = 15°$ is calculated using the Eq. (3) given by Narayanan et al. [21] is as follows:

$$S_w\ (f) = \frac{LxR}{\rho x\ a} \left[\!\left[\sum_{i=1}^{N=6} \left(\frac{S_{pp}(\theta_i)+S_{pp}(\theta_{i+1})}{2}\right) \times \Delta\theta \right]\!\right] \tag{3}$$

where L is the span of the airfoil, R is the radius of the microphone array, ρ is the density of the ambient air (kgm^{-3}) and a is the speed of sound, (ms^{-1}).
The sound power level spectrum PWL assuming cylindrical radiation from a line source is determined using the Eq. (4) given by Narayanan et al.[20] is as follows:

$$\text{PWL}\ (f) = 10\log_{10} \left[\!\left[\frac{S_w(f)}{w_{ref}} \right]\!\right] \tag{4}$$

The sound power reduction level between the baseline and sinusoidal TE serrated NACA airfoils is determined using the Eq. (5) given below:

$$\Delta\text{PWL}\ (f) = 10\log_{10} \left[\!\left[\frac{S_w(f)b}{S_w(f)s} \right]\!\right] \tag{5}$$

2.4. Turbulence characterization

The classical theory of flat plate (Amiet [22] and Roger and Moreau [23]), indicates that the far-field acoustic emissions due to the interaction of a flat plate with a turbulent flow can be entirely predicted from the spectrum of the unsteady component of velocity normal to the flat plate. Hotwire anemometry is used to characterize the turbulence at the location of the airfoil's leading edge, i.e., $100\,mm$ from the nozzle exit. In airfoils, noise radiation can either occur from the leading edge or the trailing edge and these are classified as leading-edge interaction noise and trailing edge self-noise. To quantify the dominant noise radiation zone, the stream-wise velocity spectra are measured using a single wire hot wire positioned at $100\,mm$ downstream from the nozzle exit to characterize the impinging turbulence. It is observed that the measured velocity spectra showed good agreement with the von-Karman spectrum [Fig. 4] for isotropic and homogeneous turbulence with a turbulence intensity (TI) of around 3% and $12\,mm$ stream-wise integral length scale (ILS). This turbulence intensity is adequate to make the leading edge noise source dominant over the trailing edge one for the range of frequencies (i.e., low to mid frequencies, $1\ kHz$ to about $5\ kHz$) as reported by Gruber [7]. The turbulence integral length scale is determined by matching the theoretical von Karman as well as Liepmann spectra to the measured streamwise velocity spectra, assuming ideal isotropic turbulence. The comparison of the measured velocity spectra with the theoretical one must be useful to typify the flow with minimum velocity fluctuations. The measured velocity spectra showed good agreement with the von-Karman as well as Liepmann spectra for the longitudinal isotropic turbulence [Fig. 4] similar to those given in Narayanan et al. [20] and Chaitanya et al. [24], thus corroborating that the turbulence produced in the test setup is nearly isotropic. The turbulence intensity and the integral length scale at the location of the airfoil's LE (i.e., at a distance of 100 mm from the nozzle exit) are kept constant in the present experiments. The sound produced by an airfoil in a turbulent stream is due to the unsteady component of velocity normal to the airfoil and hence our primary interest in this paper is, therefore, the normal component of turbulence velocity. The integral length scale Λ_t allied with the normal velocity component responsible for the sound generation from the airfoil is inferred from the streamwise length scale as $6\ mm$. Earlier studies by Gruber [7] reported that the impinging turbulence intensity levels greater than 2% make the leading edge noise dominant over the trailing edge self-noise. A turbulence intensity of around 3% in the present experiments indicates that the far-field acoustic measurements from the airfoil comprise overall noise (i.e., leading-edge interaction as well as trailing edge self-noise).The uncertainty in the acoustic pressure measurement is within $\pm\ 0.5\,dB$, including repeatability factors. The uncertainty in the measurement of ambient temperature inside the anechoic chamber is within ± 1℃. The frequency resolution of the spectra is 48.83 Hz. The uncertainty in the measurement of velocity is within ± 1%, including repeatability factors.

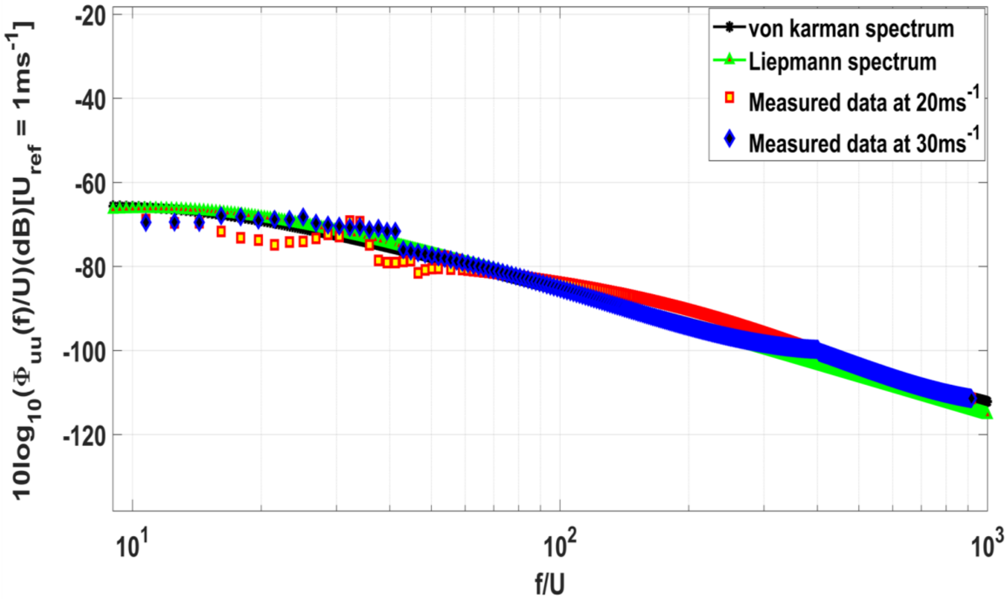

Fig.4. Comparison of the measured stream-wise velocity spectrum (ϕ_{uu}) with von-Karman and Liepmann model for longitudinal isotropic turbulence, at mean jet velocities *20 and 30* ms^{-1}.

.

3. Results and discussions

3. 1. Analytical prediction:

3.1.1. Development of an analytical model to predict the far-field noise from the serrated airfoil

The prediction of the far-field noise from a serrated airfoil of chord '*C*' and span '*y*' in a uniform stream of velocity *U* is considered by Lyu and Ayton [25], which provides an analytical solution for the TE noise using the Wiener-Hopf method as follows:

$$S_{pp}(r,\theta,y) \sim \frac{1}{4\pi r}\sin^2\frac{\theta}{2}\sum_{n=-\infty}^{\infty}\int_{-\infty}^{\infty}\prod_t(\omega,k_2)\left|\frac{\sqrt{-k_1-\kappa_n}}{k_1-\kappa_n\, cos(\theta)}E_n(-\kappa_n\, cos\,\theta)\right|^2 \mathrm{sgn}(\Re(\kappa_n))\mathrm{d}k_2 \quad (6)$$

where (r,θ,y) denotes the location of the observer in the cylindrical coordinate system *(*x/β*, y, z),* i.e. y represents the spanwise axis, θ is the polar angle in the plane formed by (x/β , z) along the x/β axis (θ = 0 represents the x/β axis) and $r = \sqrt{\left(\frac{x}{\beta}\right)^2 + z^2}$. Also,

$$\bar{h} = \frac{h}{\beta};\ k = \omega M;\ \beta = \sqrt{1-M^2};\ k_1 = \frac{\omega}{0.7};\ \overline{k_1} = \frac{k_1 + (kM - k_1M^2)}{\beta}\ ;\ \chi_n = k_2 + 2n\pi;$$

$$\kappa_n = \sqrt{\overline{k^2} - \chi_n^2}$$

$E_n(-\kappa_n \cos\theta) = \int_0^1 e^{i(\overline{k_1}-\kappa_n \cos(\theta))\overline{h}F(\eta)} e^{i2n\pi\eta} \mathrm{d}\eta$ and Π_t is the surface-pressure spectrum.

It is further simplified by replacing the integration with the summation, given by:

$$S_{pp}(r,\theta,y) \sim \frac{1}{4\pi \mathrm{r}} \sin^2\frac{\theta}{2} \frac{\overline{k_1}-\overline{k}}{\left(\overline{k_1}-\overline{k}\cos(\theta)\right)^2} \sum_{n=-\infty}^{\infty} \Pi_t(\omega, 2n\pi) \left|E_n\left(-\overline{k}\cos\theta\right)\right|^2 \quad (7)$$

where $\overline{k}$ is defined by $\overline{k} = \frac{k}{\beta}$

The surface-pressure spectrum Π_t is calculated by the Chase model in (Lyu and Ayton [25] and Chase [26]), which is given by

$$\Pi_t(\omega, k_2) = \frac{4\mathrm{TI}^2}{9\pi \mathrm{k}_\mathrm{e}^2} \frac{\widehat{k_1^2}+\widehat{k_2^2}}{\left(1+\widehat{k_1^2}+\widehat{k_2^2}\right)^{\frac{7}{3}}} \quad (8)$$

where TI = turbulent intensity and

$$k_e = \frac{\sqrt{\pi}\,\Gamma(5/6)}{L_t\,\Gamma(1/3)}; \widehat{k_1^2} = \frac{k_1}{k_e}; \widehat{k_2^2} = \frac{k_2}{k_e}$$

Though the simplified Eq. (7) has saved a great amount of computational cost as compared to that in Eq. (6) and gave results that are in good agreement with the experimental data the Chase model used to predict the wall pressure spectrum is quite outdated,

Earlier, Chase has assumed the semi-infinite rigid plate in which the radiated pressure involved the calculation of the diffraction of the short hydrodynamic waves (*U/f*) produced from the sharp edge into the sound with the larger wavelength (*c/f*). This was a nice assumption but, by considering the semi-infinite rigid plate, it shadowed the secondary leading-edge interactions which cause the third slope at higher frequencies as seen in the experiments.
Recently, Stalnov et al. [27] have extended the TNO-Blake model to predict the airfoils self-noise and developed an equation to calculate the surface pressure spectrum. The surface pressure spectrum obtained from this equation matches well with the measured spectra from mid to high range where trailing edge self-noise dominates over leading-edge interaction noise. The results obtained are in accordance with the frequencies from mid to high range where the TE noise dominates. The equation used for calculating the surface pressure spectrum in the present prediction is given by:

$$\Pi_{\mathrm{TNO}}(\omega) = \frac{4\pi\rho^2}{\Lambda_{\mathrm{p}|3}(\omega)} \int_0^\delta \Lambda_{2|22}\, U_c(x_2) \left[\frac{\partial U_1(x_2)}{\partial x_2}\right]^2 \frac{\overline{u_2^2}(x_2)}{U_c^2(x_2)} \Phi_{22}\left(\frac{\omega}{U_c(x_2)}, k_3 = 0\right) e^{-2|k|x_2} \mathrm{d}x_2 \quad (9)$$

where, $\Lambda_{2|22}$ is turbulent length scale, $\Lambda_{\mathrm{p}|3}$ is the spanwise correlation length, U_c is the convective velocity of each point x_2 inside the boundary layer and $\Phi_{22}(k_1, k_3 = 0)$ is the normalized vertical velocity spectrum which is given by:

$$\Phi_{22}(k_1, k_3 = 0, \beta_1, \beta_3) = \frac{4}{9\pi}\frac{\beta_1\beta_3}{k_e^2}\frac{\left(\frac{\beta_1 k_1}{k_e}\right)^2}{\left(1+\left(\frac{\beta_1 k_1}{k_e}\right)^2\right)^{\frac{7}{3}}}$$

$$k_e(x_2) = \frac{\sqrt{\pi}}{\Lambda_{11|1}(x_2)}\frac{\Gamma(5/6)}{\Gamma(1/3)}$$

where, $\Lambda_{11|1}(x_2)$the longitudinal integral length scale and $\beta_1, \beta_2, \beta_3$ are the stretching factors given by $\beta_1 = 1$, $\beta_2 = \frac{1}{2}$, $\beta_3 = \frac{3}{4}$. Assuming the isotropic condition, the longitudinal integral length scale is related to the transverse length scale by $\Lambda_{11|1}(x_2) = 2\,\Lambda_{2|22}(x_2)$.

As we can see, the surface pressure spectrum derived by Stalnov et al. [27] is independent of the span-wise wavenumber ($k_2 = 0$). Hence to get accurate predictions, we need to incorporate the dependence of the span-wise wavenumber (k_2) in the surface pressure spectrum model. Roger and Moreau [28] have achieved this by introducing the spanwise correlation length (l_y) given by:

$$P_w(\omega, k_2) = \frac{1}{\pi}\prod\nolimits_{TNO}(\omega)\, l_y(\omega, k_2) \tag{10}$$

where, P_w is the wall-pressure wave-number spectral density, and y is the spanwise correlation length defined as Moreau and Roger [29]:

$$l_y(\omega, k_2) = \frac{\frac{\omega}{(b_c U_c)}}{k_2^2+\left(\frac{\omega}{(b_c U_c)}\right)^2}$$

By replacing the Chase Surface Pressure model in Eq. (7) with the modified TNO-Blake model in Eq. (10), we get the following equation,

$$S_{pp}(r, \theta, y) \sim \frac{1}{4\pi r}\sin^2\frac{\theta}{2}\frac{\overline{k_1}-\overline{k}}{\left(\overline{k_1}-\overline{k}\cos(\theta)\right)^2}\sum_{n=-\infty}^{\infty}\prod\nolimits_{TNO}(\omega)\left|E_n\left(-\overline{k}\cos(\theta)\right)\right|^2 \tag{11}$$

since $\prod_{TNO}(\omega)$ is independent of the wavenumber along the spanwise direction, we can move this term outside the summation part which gives Eq. (12)

$$S_{pp}(r,\theta,y) \sim \frac{1}{4\pi^2 r} sin^2 \frac{\theta}{2} \frac{\overline{k_1}-\bar{k}}{\left(\overline{k_1}-\bar{k}\, cos(\theta)\right)^2} \prod\nolimits_{\mathrm{TNO}}(\omega) \sum_{n=-\infty}^{\infty} \left| E_n\left(\overline{-k}\, cos(\theta)\right)\right|^2 \quad (12)$$

The equation derived is similar to the one obtained by Moreau et al. [30]
By using the modified TNO-Blake model, it gives three advantages to Eq. (12) over Eq. (7)

(1) Firstly, it incorporates the secondary leading-edge interactions that were missing in the Chase model, making our predictions even more accurate for the far-field noise.

(2) Further, the spanwise correlation length is included in Eq. (12), which takes care of the spanwise variations in the far-field noise prediction of the sinusoidal serrated airfoil.

(3) With the introduction of the modified TNO-Blake model, we can get more accurate TE noise predictions at a much lower computational time.

The analytical predictions are fairly accurate since the profile/parameters of NACA 65(12)-10 airfoil, used in the present study are taken from the XFOIL data. The mathematical formula $C(y) = C_0 + h \sin(2\pi y/\lambda)$ is used to design and develop the TE serrated airfoils. The same formula is used in the analytical predictions, where C_0 is the mean chord and y is the span-wise distance also is taken into consideration to carry out the analytical prediction.

The analytical predictions are done with the help of the Trailing Edge Noise Model (TNO). The anisotropic turbulence is taken care of by introducing the stretch factors. In the TNO model, we have assumed that the surface pressure fluctuations are the same for all the serrated airfoils since we need measured boundary layer parameters as input for predicting the surface fluctuations but here we predicted the boundary layer parameters using XFOIL data and hence due to this there is some variance between the experimental data and the predicted one, however, the predictions are reasonably accurate and can benefit the readers working in the area to get a rough idea about the noise emissions from the TE serrated airfoils prior to the design and development of the next generation low noise airfoils.

3. 2. Validation:

3.2.1. Baseline airfoil

The model developed above is validated with the experiments performed on NACA 65(12)-10 airfoil in the test facility described above. To check the improvement in the revised model, it is compared with Lyu and Ayton's model [Fig 5] for the baseline airfoil. The parameters required for the prediction of surface pressure fluctuations using the TNO model are obtained from the XFOIL software at point C_0 Eq. (1) and are used for all the calculations. The validation has been done for two freestream velocities viz 30 and 40 ms^{-1}., which are compared in [Fig. 5a] and [Fig. 5b] respectively.

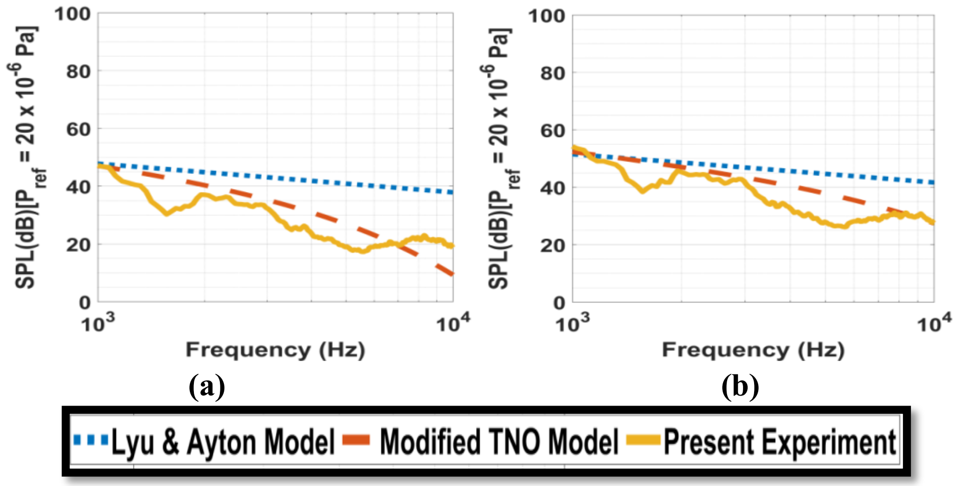

Fig. 5. The sound pressure level comparison of the Lyu and Ayton model with the modified TNO model for baseline w.r.t present experiment for (a) *30* ms^{-1} (b) *40* ms^{-1} respectively.

It can be observed that by the incorporation of the modified TNO model in calculating the surface pressure spectrum, there is a significant improvement in the prediction of the far-field spectra as compared to the model proposed by Lyu and Ayton [25]. The model is now able to predict the far-field noise, especially at higher frequencies where the TE noise dominates over the LE ones. The deviations from the experimental results for both models are shown in [Fig. 5a] and [Fig. 5b] for *30 and 40* ms^{-1} respectively. For the major part of frequencies, the standard deviation of the spectra of the models is lies within the range of $\pm$ *4* dB, within the frequency range of our interest. For the major part of frequencies, the deviation lies within about $\pm$ *4* dB.

The analytical predictions are done with the help of the Trailing Edge Noise (TNO) Model. The anisotropic turbulence is taken care of by introducing the stretch factors. In the TNO model, we have assumed that the surface pressure fluctuations are the same for all the serrated airfoils since we need measured boundary layer parameters as input for predicting the surface fluctuations near the trailing edge but here we predicted the boundary layer parameters using XFOIL data and hence due to this there is some variance between the experimental data and the predicted one, however, the predictions are reasonably accurate and can benefit the readers working in the area to get a rough idea about the noise emissions from the TE serrated airfoils prior to the design and development of the next generation low noise airfoils. The idea of modifying the present Weiner-Hopf method is to provide readers with a tool to calculate reasonably accurate noise emissions from the TE serrations. This is done with the help of the Trailing Edge Noise (TNO) Model to calculate the surface-pressure spectrum of the airfoil near the trailing edge. A comparison is made between the Lyu & Ayton Model and the modified TNO Model and is shown in [Fig. 5]. With the modifications, the model can now more precisely capture the far-field spectrum as compared with the previous model.

3.2.2 Comparison of the far-field noise spectra and reductions obtained from predictions and experiments:

The results obtained from Eq. (12) are compared directly with the experimental data. The data is plotted for two different uniform jet velocities i.e. $30 \text{ and } 40\ ms^{-1}$ at a radius, $r = 0.65\ m$. As observed from the experimental data, the serration showing the highest reductions for $\lambda/C_0 = 0.2$, $h/C_0 = 0.1667$ at $\theta = 90^o$ (i.e. the observer is directly above the airfoil's trailing edge) is chosen and plotted in [Fig. 5].. For both velocities, it is observed that the spectral shape is well captured by the predictions. It is well known that the jet noise dominates at low frequencies and leading-edge interaction noise dominates from low to mid-frequency ranges. Also, from mid to high frequency ranges the trailing edge noise starts to dominate over the leading edge one. At lower frequencies, the deviations with the experiments might be due to the dominance of jet noise and interaction noise as mentioned above but as we move towards the higher frequencies.

Some deviations will always exist with the experiments because of the presence of noises due to other major sources such as the jet noise and vortex pairs, which form interference peaks and eventually gives rise to the scattered experimental data. To get a clear picture of the accuracy of the modified TE noise model devised above, we need to eliminate the scattering of the experimental data. This can somehow be achieved by comparing the differences in the SPL spectra ΔSPL of baseline with serration for both, the predictions and the experiments. $\Delta\text{SPL}_{Analytical}$ is calculated using the formula:

$$\Delta\text{SPL}_{Analytical} = SPL_{Analytical\ Baseline} - SPL_{Analytical\ Serration} \tag{13}$$

From [Fig. 6], the r.m.s $\Delta\text{SPL}_{Analytical}$ is within about $\pm\ 4\ dB$ band w.r.t. the $\Delta\text{SPL}_{Experimental}$ for a wide range of frequencies. Thus, it reveals that with the use of a modified TNO model along with the TE far-field noise equations derived using the Wiener-Hopf method, we can get more accurate ΔSPL predictions.

(A)

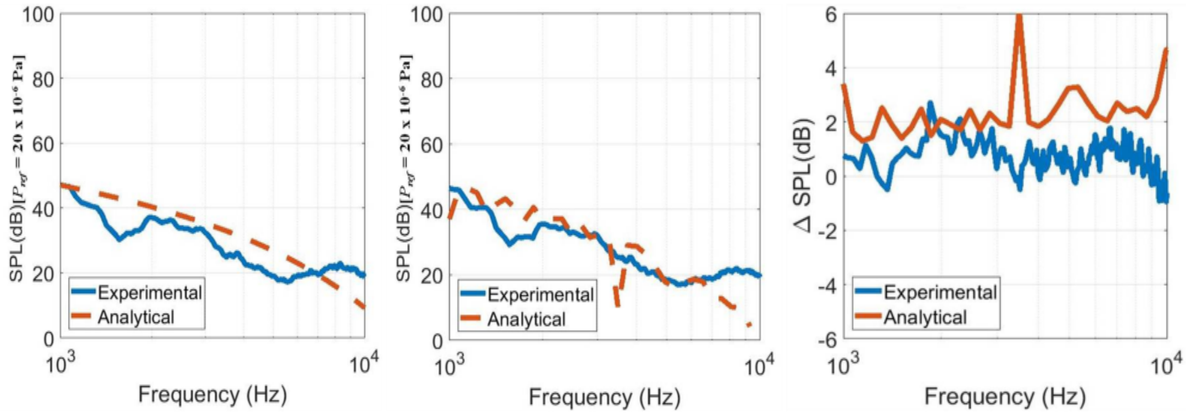

(a) **(b)** **(c)**

(B)

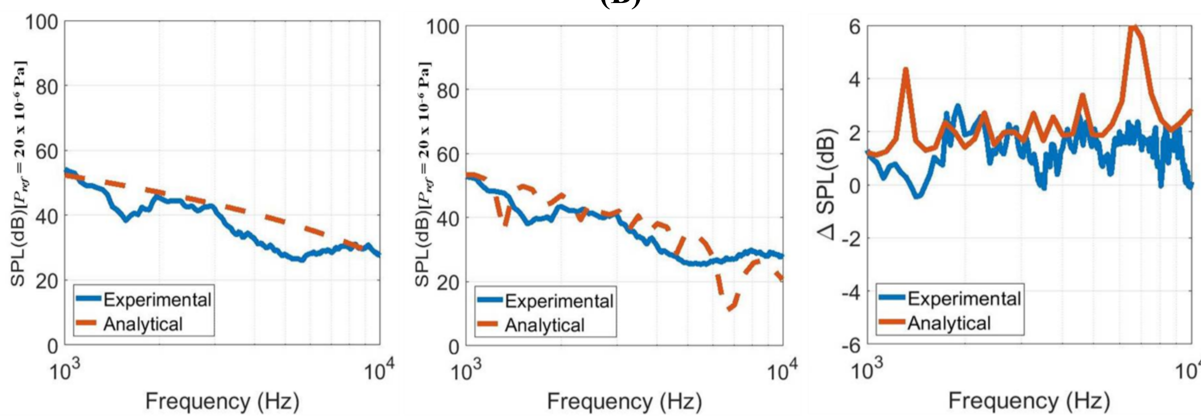

(d) **(e)** **(f)**

Fig. 6. Comparison of predicted SPL and ΔSPL with experimental SPL and ΔSPL for $\lambda/C_0 = 0.2$, $h/C_0 = 0.1667$ for (a,d) Baseline (b,e) serration (c,f) ΔSPL at 2 different velocities (A) $30\ ms^{-1}$ (B) $40\ ms^{-1}$.

In general, the spectral shape is well captured by the predictions for both the jet velocities. It is well known that the jet noise dominates at low frequencies and leading-edge interaction noise dominates from low to mid-frequency ranges. Also, from mid to high frequency ranges the trailing edge noise starts to dominate over the leading edge one. At lower frequencies, the deviations with the experiments might be due to the dominance of jet noise/interaction noise but as we move towards the higher frequencies, the predictions come in close agreement with the experiments.

The discrepancies observed in the calculations [Fig. 6] can be associated with the given three reasons.

1. Using experimental data for surface-pressure spectrum: The boundary layer values used in

the TNO model are calculated with the help of XFOIL. It is assumed that the values remain constant irrespective of the TE serration used but in actuality, this cannot be true.

2. TE noise interference on the overall noise spectra: As observed from the later work in the paper, noise radiations from TE serrations do interfere with the LE noise and hence the overall noise spectra. However, in the current modification, it is not incorporated due to difficulty.
3. The shear layer correction effects on the far-field noise are not included in the present modifications since it makes the problem more complicated. Further, the shear layer correction effects may be significant at higher jet velocity, that is why the deviation between the present predictions and the experiments are higher at higher jet velocity (Fig. 6 (c) as compared to Figs. 6 (a) and (b).

The present predictions may be improved if all the above-mentioned can be incorporated, however, it is for future work as it will deviate the scope of the current paper. Some deviations will always exist with the experiments because of the presence of noise due to other major sources such as the jet noise and vortex pairs, which form interference peaks and eventually gives rise to the scattered experimental data.

3.2.3. Analytical approach on the effect of serration amplitude (h) on the TE noise:

As observed from the experimental results given in Section 4.1.3, the noise reductions can be increased by increasing the serration amplitude, *h*. However, observing the effect of *h*, specifically on TE noise, cannot be seen clearly as the experimental data is mixed with other noises such as the jet noise, leading-edge noise, and vortex pairs. The high accuracy of Eq. (12) in predicting the TE noise makes it a good approach to examine the effect of *h* for the same serration wavelength.

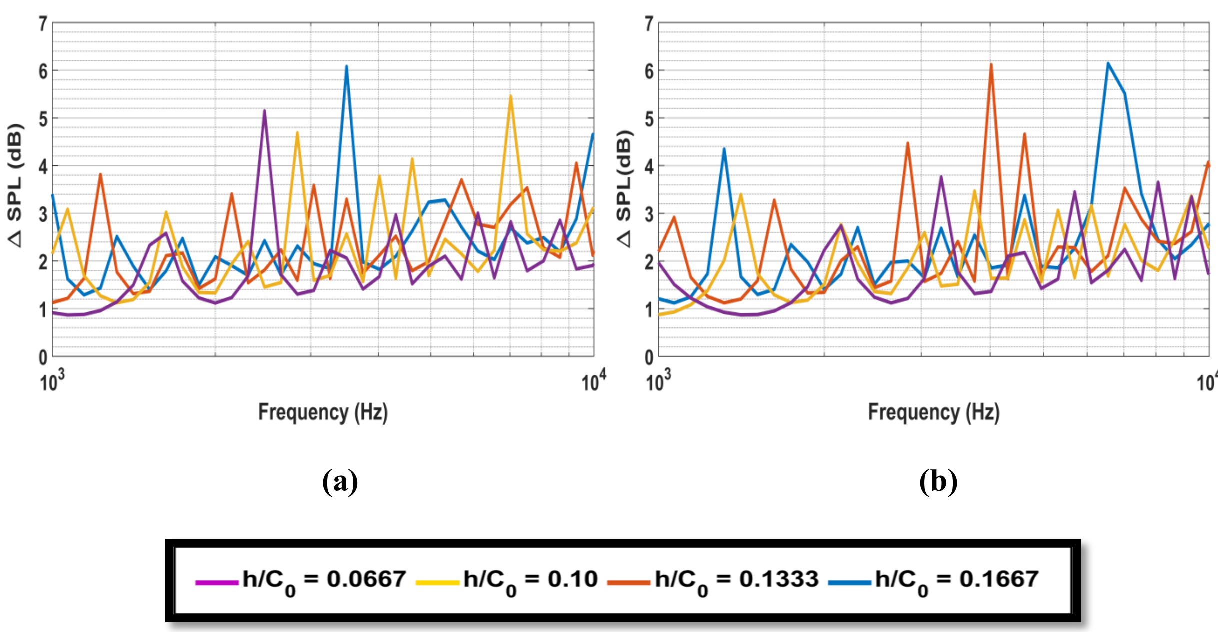

(a) **(b)**

Fig.7. Analytical comparison of predicted far-field TE noise for different h/C_0 and $\lambda/C_0 = 0.2$ at (a) $30\ ms^{-1}$ (b) $40\ ms^{-1}$.

The predicted far-field TE noise reductions at $\lambda/C_0 = 0.2$ and different serration amplitudes are shown in [Fig. 7], for different jet velocities of $30\ ms^{-1}$ and $40\ ms^{-1}$. In general, all the TE serrations are providing significant noise reductions from about 2 kHz onwards which indicates the efficacy of sinusoidal TE serrations in reducing broadband noise. It is observed that longer amplitude serrations i.e. for higher h/C_0, showed the highest noise reductions for both the jet velocities. Also, the striking feature observed is that the frequency at which the highest noise reduction provided by the longest serration shifts to a higher value for a higher jet velocity of $40\ ms^{-1}$. As h decreases it is seen that the maximum noise reductions provided by the serration shift to mid-frequency from higher one and this behavior are observed for both the jet velocities. At the maximum noise reduction zone, the noise reductions are observed to decrease with a decrease in h values, which reveals that the longer serrations could provide higher noise reductions as compared to shorter ones, thus corroborating the experimental findings. This behavior is observed at the mid-frequency range for a jet velocity of $30\ ms^{-1}$ and the high-frequency range for a jet velocity of $40\ ms^{-1}$. Thus, theoretical prediction reveals that the highest reductions provided by the TE serrations are observed from mid to high-frequency ranges as compared to the low-frequency range. [Fig. 7] shows the variations in the noise reduction level w.r.t reference line ($0\ dB$) since the values above the reference line show the noise reduction level while the values below it show the noise enhancement level. Hence, we conclude from the figure that the maximum noise reduction zone is found to be at the self-noise region.

4. Experimental spectral results

4.1. Spectral features

4.1.1. Acoustic spectra comparison of sinusoidal and triangular TE serrations

The spectra shown in the paper are based on far-field acoustic measurements of the overall noise radiated (i.e., leading-edge interaction noise + trailing edge self-noise) from the baseline and TE serrated airfoils. The sound power level spectra of the sinusoidal i.e., wavy TE serrations with $\lambda/C_0 = 0.0333$, $h/C_0 = 0.1667$ and $\lambda/C_0 = 0.1667$, $h/C_0 = 0.1667$ introduced at the trailing edge of a NACA airfoil are compared with triangular i.e., v-serrated ones for the same parametric conditions in[Fig. 8] at the jet velocity of $40\ ms^{-1}$, to understand the efficacy of the sinusoidal TE serrations over triangular ones. It is observed that the sinusoidal i.e., wavy TE serrations (solid red curve) showed lower far-field acoustic emissions as compared to v-serrations (solid blue curve) over a wide range of frequencies from about $0.5\text{-}10\ kHz$. In general, it is observed that the far-field acoustic radiations from the sinusoidal TE serrations are lower than v-serrations for the range of frequencies from about *0.5-10 kHz* as well as *15-20 kHz*, irrespective of the jet velocities. It reveals that the sinusoidal TE serrations could effectively reduce the far-field acoustic emissions as compared to the v-serrations. Also, for all the jet velocities studied, the far-field acoustic emissions of the sinusoidal TE serrations are observed to be much lower than the v-serrations for the frequencies from about *4-10 kHz*. Thus, the present study indicates that the sinusoidal serrations could effectively reduce trailing edge self-noise which generally arises at high frequencies (i.e., > *5 kHz*) as reported by Sivakumar et al. [12]. In general, it is noticed that the wider sinusoidal TE serrations [Fig. 8b] generate lower overall acoustic emissions as compared to narrow ones [Fig. 8a] for the range of frequencies from about *0.5-10 kHz*, at all jet velocities studied.

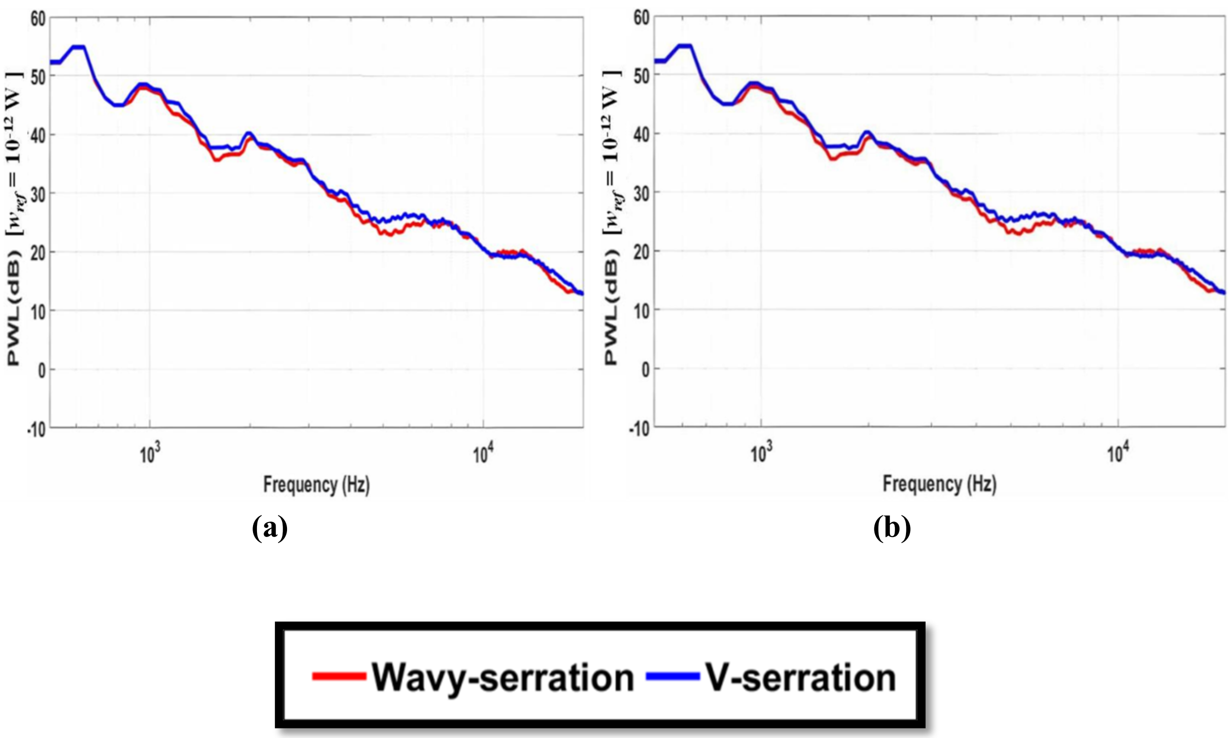

Fig.8. Acoustic spectra comparison of sinusoidal and v-serrated NACA airfoil at $h/C_0 = 0.1667$ (a) $\lambda/C_0 = 0.0333$ and (b) $\lambda/C_0 = 0.1667$, for a jet velocity of $40\, ms^{-1}$.

.

The probable reason for the lower far-field noise emissions provided by the sinusoidal TE serrations may be due to the presence of weak compact root sources as a result of the smooth mixing of the upper and lower boundary layers at the root of the sinusoidal serrations, which reduces the edge scattering and hence the far-field noise as compared to the v-serrations. Thus, it demonstrates that the sinusoidal serrations act as the best passively modified TE profiles for achieving significant reductions of the overall noise as well as trailing edge self-noise as compared to v-serrations.

4.1.2. Sound pressure spectra comparison of baseline NACA airfoil, and TE serrated NACA airfoils

Typical acoustic spectra of overall far-field noise from baseline NACA airfoil and sinusoidal i.e., wavy trailing edged NACA airfoils are compared in [Fig. 9] at $U = 30\ ms^{-1}$, for all TE amplitudes h/C_0 at a fixed λ/C_0 value of 0.1667.

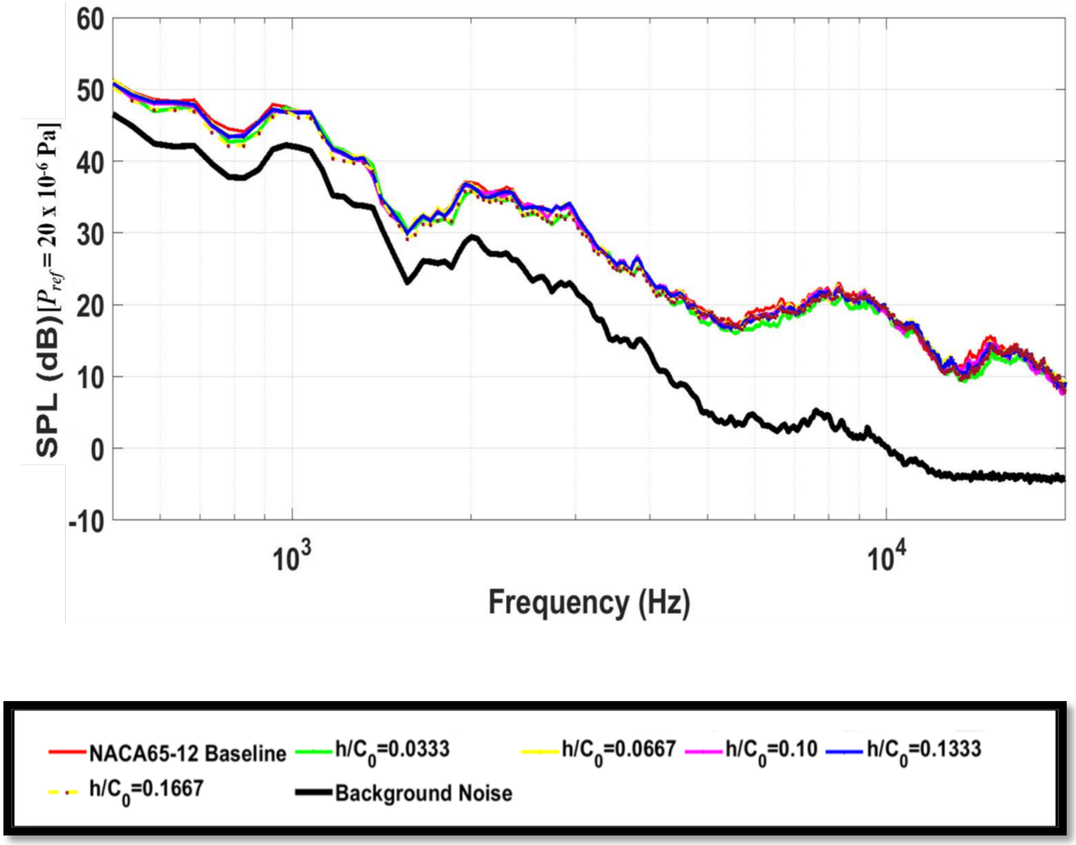

Fig.9. Typical acoustic spectra comparison of baseline NACA airfoil and TE serrated NACA airfoils at a λ/C_0 value of 0.1667 and h/C_0 values of 0.0333, 0.0667, 0.10, 0.1333, 0.1667, for a jet velocity of $30\ ms^{-1}$.

The paper emphasizes the substantial reductions of the far-field acoustic emissions for the range of frequencies from about $4\text{-}10\ kHz$, from the overall broadband noise measurements. The leading edge interaction noise is the dominant one as compared to the trailing edge self-noise due to impinging turbulence intensity $> 2\%$ in the present experiments as mentioned earlier. The background noise measured at the same jet velocity [Fig. 9] is observed to be significantly lower than the overall acoustic radiations from the realistic airfoils, which indicates that the background noise does not affect the far-field acoustic radiations from the baseline and serrated foils. The background noise measurements are made with the jet flow in the presence of side plates but without airfoil. The considerable noise reductions of about $2\,dB$ are limited to the frequencies from $4\text{-}10\ kHz$, where the trailing edge self-noise dominates over the leading edge interaction noise.

A striking feature of the sound pressure spectra obtained with sinusoidal TE serrations is that the far-field acoustic emission levels in the spectra obtained with the baseline for the range of frequencies from about $4\text{-}10\ kHz$ are much reduced, while the characteristic oscillations are not reduced. Unlike leading-edge serrations, the pressure jump along the span and across the chord is nearly coherent due to the reduced scattering of the pressure by the sinusoidal TE serrations. The probable reason for the reduction in the scattering of the pressure by the serrated TE may be due to the presence of weaker surface pressure fluctuations than the serration peaks as a result of the smooth mixing of the upper and lower boundary layers at the root of the serrations. The interference peaks as shown in [Fig. 9] are not suppressed like those observed for leading-edge serrations are given in Narayanan et al. [20], while the peaks shift to a lower level thus reducing the far-field acoustic emissions. It also shows that the far-field acoustic emission levels decrease with a decrease in the amplitude of the sinusoidal TE serration for a fixed λ/C_0 value of 0.1667 for the range of frequencies from about $0.5\text{-}10\ kHz$, while much-reduced emission levels are noticed for the range of frequencies from about $4\text{-}10\ kHz$. Thus, it reveals that the shorter sinusoidal TE serrations generate lower far-field acoustic emissions as compared to the longer ones for a fixed value of λ/C_0.

4.1.3. Sound power level spectra comparison of baseline and serrated- NACA-65 airfoils

The sound power spectra of baseline and sinusoidal TE serrated airfoils at a fixed λ/C_0 value of 0.0333 and h/C_0 values of 0.0333, 0.0667, 0.10, 0.1333, 0.1666 are shown in the right-hand side of [Fig. 10].

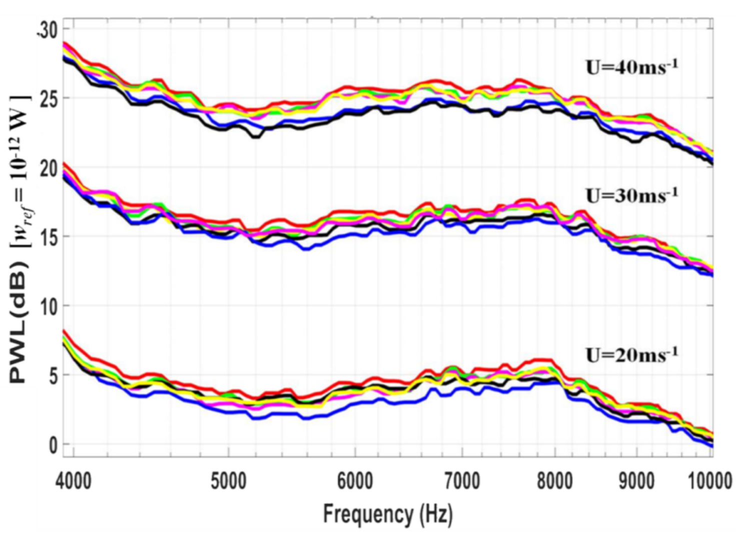

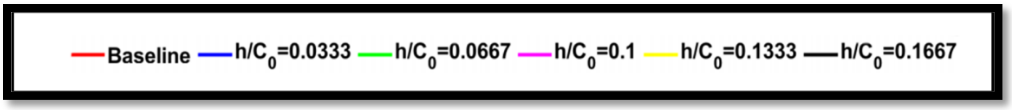

Fig.10. Sound power level spectra comparison of baseline and TE serrated NACA airfoils at $\lambda/C_0 = 0.20$ and different h/C_0 values for various jet velocities

It is observed that the far-field acoustic radiations of the baseline TE serrated NACA airfoil with $\lambda/C_0 = 0.0333$ and $h/C_0 = 0.0667$ are almost the same for a certain range of frequencies and jet velocities. In general, it is observed that the baseline NACA airfoil radiates higher far-field noise for the entire range of frequencies from $4\text{-}10\ kHz$ as compared to the TE serrated airfoils except for the serrated one with $\lambda/C_0 = 0.0333$ and $h/C_0 = 0.0667$ as mentioned above. It is observed that the sinusoidal TE serrated NACA airfoil obtained with $\lambda/C_0 = 0.0333$ and $h/C_0 = 0.0333$, generates the lowest far-field acoustic radiations for the range of frequencies from $4\text{-}10\ kHz$, as compared to other TE serrated NACA airfoils. Further, it reveals that the far-field acoustic radiations are observed to decrease with an increase in h/C_0 value from 0.0667 to 0.1666, for the range of frequencies from $4\text{-}10\ kHz$, except for the smallest h/C_0 value of 0.0333, which showed the lowest emission levels as mentioned above. Also, the far-field acoustic radiations of the baseline and sinusoidal TE serrated NACA airfoils are observed to increase with the increase in jet velocities. Thus, it reveals that h/C_0 values play a crucial role in modifying the far-field acoustic radiations when compared to a fixed λ/C_0 value of 0.0333, for all the jet velocities. The lower far-field radiations provided by the sinusoidal serrated TE airfoil may be due to the presence of weaker surface pressure fluctuations in the vicinity of the TE as a result of the reduced velocity fluctuations in the vertical cross-section close to the TE as reported by Tang et al. [31]. Further, the surface pressure fluctuations are primarily concentrated at the peaks of the sinusoidal TE serrations rather than disseminated throughout the span of the straight edge baseline airfoil. Thus, it reveals that the radiation of weaker surface pressure fluctuations primarily from the peaks of the sinusoidal TE serrations results in the reduced far-field noise as compared to the straight edge baseline where the intense surface pressure fluctuations throughout the span of the airfoil radiate to the far-field. The noise reductions provided by the sinusoidal TE serrated NACA airfoils are given in the following section.

5. Sound power reduction levels

5.1. Sound power reduction levels (ΔPWLs) of sinusoidal TE serrated NACA-65 airfoils

The sound power level reduction levels (ΔPWLs) of TE serrated NACA airfoils at $\lambda/C_0 = 0.0333$ and 0.2 for different h/C_0 values are compared in [Fig. 11] at three different jet velocities.

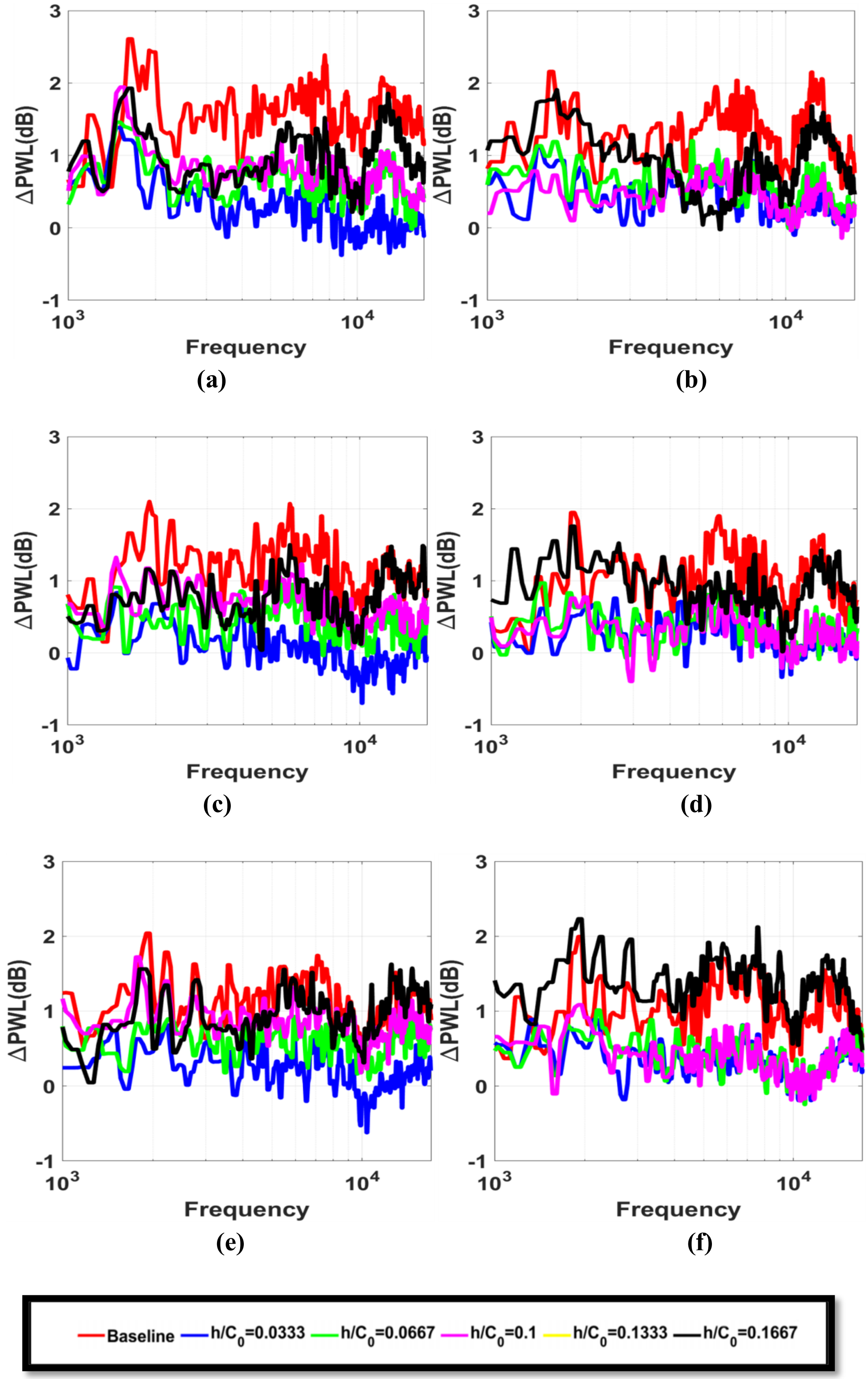

ΔPWL(dB)
Frequency
(a)
(b)
(c)
(d)
(e)
(f)
Baseline
h/C0=0.0333
h/C0=0.0667
h/C0=0.1
h/C0=0.1333
h/C0=0.1667

Fig.11. Sound Power Level Reduction (ΔPWL) comparison for) $\lambda/C_0 = 0.033$ shown in (a, c, e) and $\lambda/C_0 = 0.2$ shown in (b, d, f) at different jet velocities of $20, 30$ *and* $40\ ms^{-1}$ resp.

It is observed that the sound power reductions are highest (i.e., about $2\ dB$) for the smallest h/C_0 value of 0.0333 (i.e., smallest amplitude serration) for the range of frequencies from $1\text{-}15\ kHz$. Also, another noteworthy feature observed for the range of frequencies from $5\text{-}10\ kHz$ is that the noise reduction decreases with a decrease in h/C_0 values, whilst the highest reductions are seen for the smallest h/C_0 value of 0.0333 as mentioned above. Similar behaviors are observed for all jet velocities studied. Further, it reveals that the noise reduction decreases with an increase in jet velocities for all h/C_0 values. At high frequencies from $10\text{-}15\ kHz$, the noise reductions of the shorter serration (i.e., $h/C_0 = 0.0333$) are slightly higher than longer one (i.e., $h/C_0 = 0.167$) at a jet velocity of $20\ ms^{-1}$, while at higher jet velocities the noise reduction provided by the shorter and longer serrations are the same. Similarly, the noise reductions provided by the serrations with $h/C_0 = 0.10$ and $h/C_0 = 0.1333$ are also the same, for the range of frequencies from 10 *to* $15\ kHz$, while the lowest noise reduction is provided by the serration having an h/C_0 value of 0.0667.
At a higher λ/C_0 value of 0.2, higher sound power reductions of about $2\,dB$ and $1.5\,dB$ are observed at smallest and largest h/C_0 values of 0.0333 and 0.166, for the range of frequencies from about $4\text{-}12\ kHz$ and $7\text{-}15\ kHz$ at jet velocities of 20 *and* $30\ ms^{-1}$. Also, it is observed that the noise reductions of about $2\ dB$ provided by the smallest and largest h/C_0 values of 0.0333 and 0.166 are almost the same at a higher jet velocity of $40\ ms^{-1}$ and are observed for the range of frequencies from $1\text{-}15\ kHz$. For all the jet velocities, the sinusoidal TE serrated airfoils with h/C_0 values of 0.0667, 0.10, and 0.1333 provided lower noise reductions of about 0.5 *to* $1\ dB$ for the range of frequencies from $1\text{-}15\ kHz$. Thus, the present study demonstrates that the highest noise reductions could be achieved with both the narrow - shorter serrations as well as wider - shorter serrations. The longer and shorter serrations are based on amplitudes while wider and narrow serrations are based on the wavelengths. The sinusoidal TE serrations with wavelengths (λ/C_0) of $0.0333, 0.0667, 0.10, 0.1333, 0.2$ and amplitudes (h/C_0) of $0.0333, 0.0667, 0.10, 0.1333,$ and 0.1667 are been compared. The longer and shorter serrations based on amplitude are 0.0333 and 0.1667 respectively *and* wider and narrow serrations based on the wavelengths are 0.0333 and 0.2 are as follows.

Subsequently, it also reveals that the higher noise reductions are possible with the narrow - longer serrations as well as wider - longer serrations. The probable reason for the reductions in the overall far-field noise provided by the sinusoidal TE serrations may be due to the reductions in the surface pressure fluctuations near the serrated trailing edge as a result of the reduced vertical velocity fluctuations as reported by Tang et al. [31]. It also reveals that the surface pressure fluctuations are primarily concentrated at the tip of the TE serrations but the surface pressure fluctuations occur throughout the span of the straight edge baseline airfoil. The surface pressure fluctuations concentrated at the tip of the sinusoidal TE serrations primarily lead to the far-field acoustic radiations, while the surface pressure fluctuations throughout the span of the baseline airfoil radiate to the far-field, which results in the weak acoustic radiations from the sinusoidal TE serrated airfoils as compared to baseline airfoil. The acoustic radiations from the subsequent serrated tips interfere incoherently and reduce the airfoil self-noise. The generation of weak acoustic radiations from the tip of the sinusoidal TE serrations propagate upstream and interfere destructively with the strong radiations emanated from the leading edge, thus creating a feedback loop between the upstream propagating acoustic waves from the TE with the strong leading-edge radiations and reduces the leading edge noise along with the self-noise, which results in the reductions of the overall noise in the far-field. The reductions of the overall noise along with the trailing edge self-noise which dominates from mid to high-frequency range demonstrate the establishment of the feedback loop and far-field interference with the noise radiated from the TE with the LE. It also portrays that the TE modifications could modify the far-field interference effects for a wide range of frequencies without modifying the flow field near the leading edge of the airfoil.

The presence of a feedback loop is evident from the directivity plots given in *Section 7.1*. One of our earlier papers Chaitanya et al. [24] showed that the sinusoidal leading-edge serrations can also reduce the trailing edge self-noise, thus confirming the effectiveness of the sinusoidal serrations (i.e., leading/trailing) in controlling the leading edge interaction noise along with trailing edge self-noise. The present paper shows the efficacy of sinusoidal trailing-edge serrations in reducing the overall noise by reducing the leading edge interaction noise along with trailing edge self-noise.

6. Overall noise reduction characteristics

6.1. Overall sound power reduction levels of sinusoidal TE serrated NACA-65 airfoils

The overall sound power reduction level ΔOAPWL comparison of TE serrated NACA airfoils with λ/Λ_t for various h/C_0 values is shown in [Fig. 12] at jet velocities of *20, 30 and 40* ms^{-1}, where λ is the serration wavelength and Λ_t is the transverse integral length scale(mm). The ΔOAPWL is calculated for the range frequencies from *0.1-10* kHz and *4-10* kHz. The overall sound power level OAPWL(f) is determined by integrating the sound power for the range of frequencies from *0.1-10* kHz and *4-10* kHz as given in Eq. (14).

$$\text{OAPWL}(f) = 10\log_{10}\left[\!\left[\sum_{i=1}^{n}\left(\frac{w(f_i)}{w_{ref}}\right)\right]\!\right] \qquad 0.1 < f_i < 25\ kHz \tag{14}$$

where $w(f_i)$ is the sound power in Watts and $w_{ref} = 10^{-12}\ W$. The sound power reduction level ΔOAPWL (f) is determined using the Eq. (15) given below

$$\Delta\text{OAPWL}(f) = 10\log_{10}\left[\!\left[\sum_{i=1}^{n}\left(\frac{w(f_i)\text{b}}{w(f_i)\text{s.}}\right)\right]\!\right] \tag{15}$$

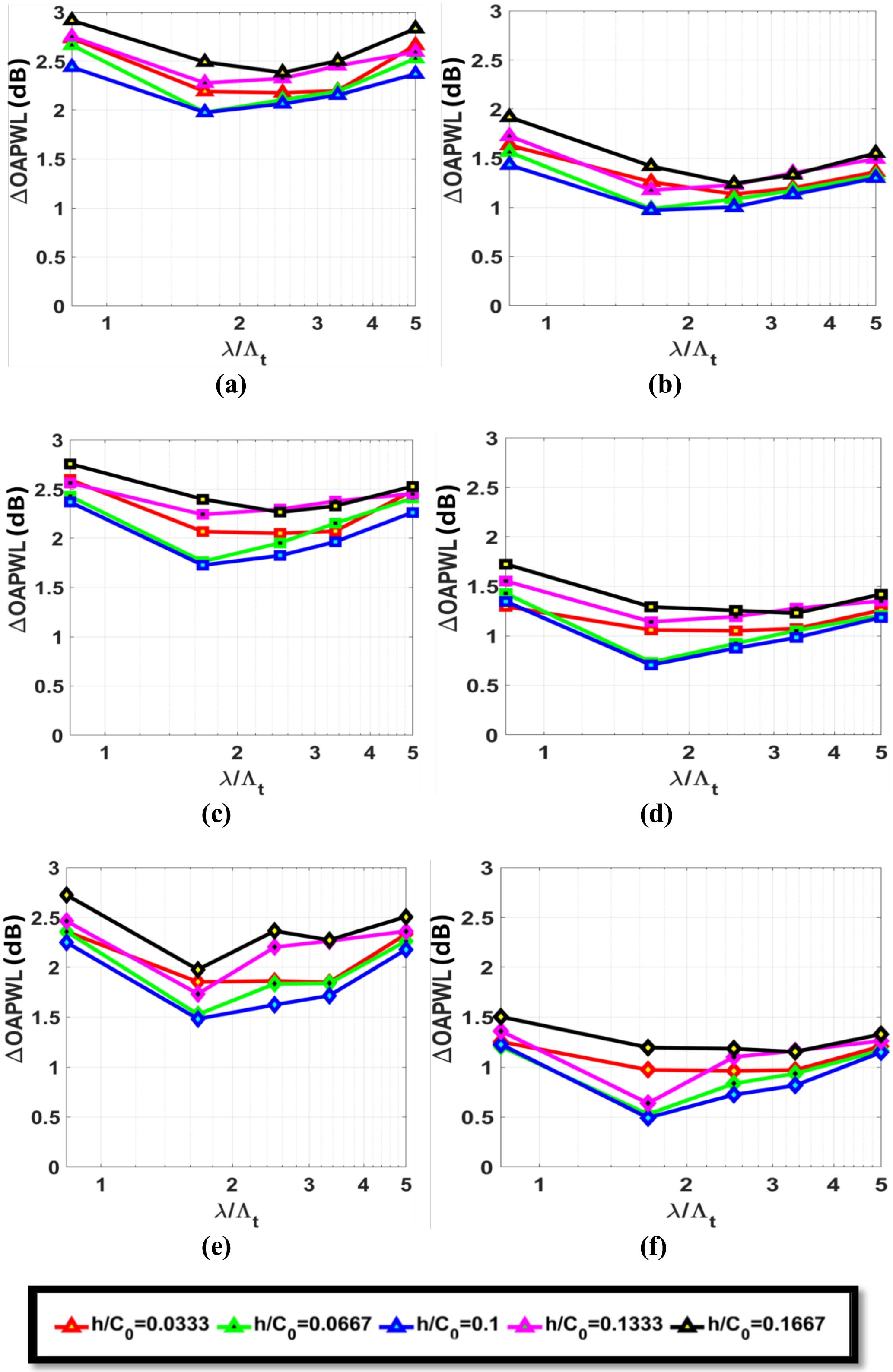

Fig.12. Variation of ΔOAPWL with λ/Λ_t for different serration amplitudes h/C_0 for the various frequency ranges i.e. (a, c, e) *0.1-4kHz* and (b, d, f) *4-10kHz* for jet velocity $20\ ms^{-1}$, $30\ ms^{-1}$ and $40\ ms^{-1}$ resp.

For all the jet velocities studied, the lowest noise reduction of about 2 and $1\,dB$ is observed at λ/Λ_t = *1.67* for the range of frequencies 0.1-$10\ kHz$ and 4-$10\ kHz$ and the noise reductions increases on either side of λ/Λ_t = *1.67* for all h/C_0 values. It reveals that the longer serrations provide higher noise reductions for all the λ/Λ_t values and the highest noise reductions are seen for the λ/Λ_t values of *0.833* and *5*, which are observed to be independent of jet velocities. Also, it shows that higher noise reductions are possible with longer/narrow as well as longer/wider serrations. The present investigation shows that h/C_0 is a crucial parameter in controlling the interaction as well as self-noise reductions as compared to the λ/C_0. Thus, the present study demonstrates that the presence of sinusoidal trailing edge serrations in airfoil could effectively control the high-frequency self-noise due to the reduction in the surface pressure fluctuations close to the trailing edge as a result of the reduced velocity fluctuations. It also shows that the control of the overall noise i.e., leading-edge interaction + trailing edge self-noise over a wide range of frequencies.

It is observed from [Fig. 12] that the local maxima are observed to occur when the transverse turbulence integral length scale is either 1.2 [i.e. 1/0.833] or 0.2 [i.e. 1/5] times the serration wavelength, which corresponds to λ/Λ_t = *0.833* or *5*. It indicates that the minimum noise reductions occur when λ/Λ_t = *1.67* and local maxima of the noise reductions occur on either side of the λ/Λ_t = *0.833* and *5*.

6.1.1. Development of an empirical expression to determine overall sound power reduction levels of sinusoidal TE serrated NACA-65 airfoils

The variation of overall sound power reductions ΔOAPWL with h/C_0 for narrow and wide serrations i.e., λ/C_0 = *0.033* and *0.2* are shown in [Fig. 13] at different jet velocities since the present study reveals that h/C_0 is the key parameter in controlling the far-field noise reductions. The ΔOAPWL is determined by integrating the sound power for the range of frequencies from 4 - $10\ kHz$ at which trailing edge self-noise dominates over interaction one and the TE serrations show significant noise reductions. It is observed that for both the λ/C_0 values, ΔOAPWL decreases with an increase in h/C_0 values, and a minimum ΔOAPWL is attained for h/C_0 values of *0.066* and *0.1* depending on the flow velocities. For both the λ/C_0 values, ΔOAPWL is observed to increase with the increase in h/C_0 beyond an h/C_0 value of *0.1* at all jet velocities studied. Regression analysis is performed to determine the ΔOAPWL for other h/C_0 values and jet velocities due to their unique behavior for both the λ/C_0 values at all jet velocities. Based on this, an empirical expression is developed to determine the ΔOAPWL and h/C_0 values, which is applicable for all the λ/C_0 values and jet velocities. The second-order poly-fit with correlation coefficient $r_c > 0.95$, strongly recommends the quadratic dependence of ΔOAPWL with h/C_0. The empirical expression obtained for the ΔOAPWL based on the second-order poly-fit is given

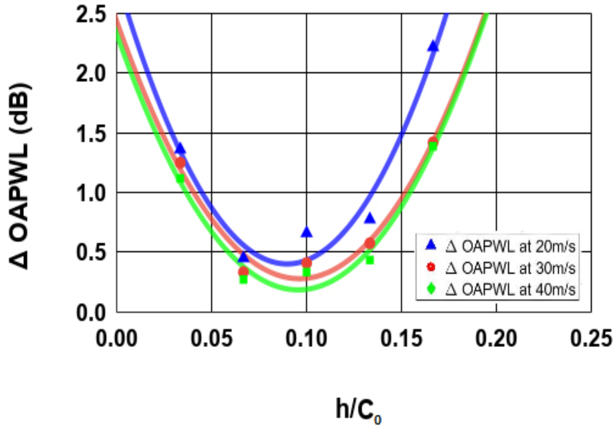

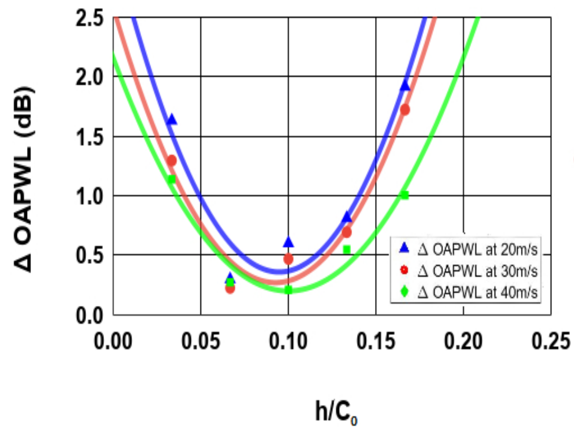

(a) **(b)**

Fig.13. Variation of overall sound power reductions (ΔOAPWL) with various h/C_0 for (a) $\lambda/C_0 = 0.0333$ (b) $\lambda/C_0 = 0.2$ at different jet velocities.

Table 1
Value of constants *a*, *b* and *c* to predict ΔOAPWL for different h/C_0 values at a λ/C_0 value of 0.033 for different jet velocities used in Eq. 15.

Velocity (ms^{-1})	*a*	*b*	*c*
20	308	-58.30	3.12
30	269	-49.80	2.58
40	196	-39.20	2.16

Table 2
Value of constants *a*, *b* and *c* to predict ΔOAPWL for different h/C_0 values at a λ/C_0 value of 0.2 for different jet velocities used in Eq. 15.

Velocity (ms^{-1})	*a*	*b*	*c*
20	297	-53.30	2.79
30	232	-44.70	2.43
40	221	-42.80	2.26

$$\Delta OAPWL = a\,(h/C_0)^2 + b\,(h/C_0) + c \quad (16)$$

where *a, b* and *c* are constants obtained from the second-order fit. The values of the constants *a, b,* and *c* at λ/C_0 values of *0.033* and *0.2* are given in Tables 1 and 2 for all the jet velocities.

6.1.2. Strouhal number scaling law for the sinusoidal trailing edge serrations

The variation of normalized sound power reduction ΔPWL' i.e., $\Delta PWL / \Delta PWL_{max}$ with modified Strouhal number, S_{thm} for smaller, intermediate, and larger λ/C_0 values of *0.0333*, *0.0667*, and *0.2* of the sinusoidal trailing edge serrated airfoils are shown in [Fig. 14] for jet velocities of *30 and 40* ms^{-1} respectively. For both jet velocities, the normalized sound power reduction spectra of the sinusoidal trailing serrated airfoils are observed to coalesce on a modified Strouhal number S_{thm} , for λ/C_0 values of *0.0333* and *0.2* [Fig. 14(a,c)] and [Fig. 14(d,f)] while no coalesce is observed for an intermediate λ/C_0 value of *0.0667* [Fig. 14b] and [Fig. 14e]. The modified Strouhal number S_{thm} is the Strouhal number obtained when it is multiplied by a constant factor $(1 + \log(\lambda/\Lambda_t))$, which depends only on the serration wavelength if the transverse integral length scale is constant. The modified Strouhal number is given as

$$S_{thm} = fh/U(1 + \log(\lambda/\Lambda_t)) = s_{th}\,(1 + \log(\lambda/\Lambda_t)) \quad (17)$$

where the Strouhal number $s_{th} = fh/U$. Thus, the present study reveals that the normalized sound power reduction ΔPWL' with modified Strouhal number S_{thm} is almost independent of jet speed. Chaitanya et al. [24] reported that sound power reduction spectra of the sinusoidal leading-edge serrated airfoils coalesce on the Strouhal number s_{th} for a certain optimum wavelength $\lambda/\Lambda_t \sim 4$ where the maximum noise reductions occur, while for the sinusoidal trailing serrated airfoils coalesce on the modified Strouhal number S_{thm} for λ/C_0 values of *0.0333* and *0.2*, where the maximum noise reductions are obtained, while coalesce is not seen for a λ/C_0 value of *0.0667*. It indicates that there exists a certain wavelength narrow or wider, $\lambda = \lambda'$ at which greater noise reductions are possible.

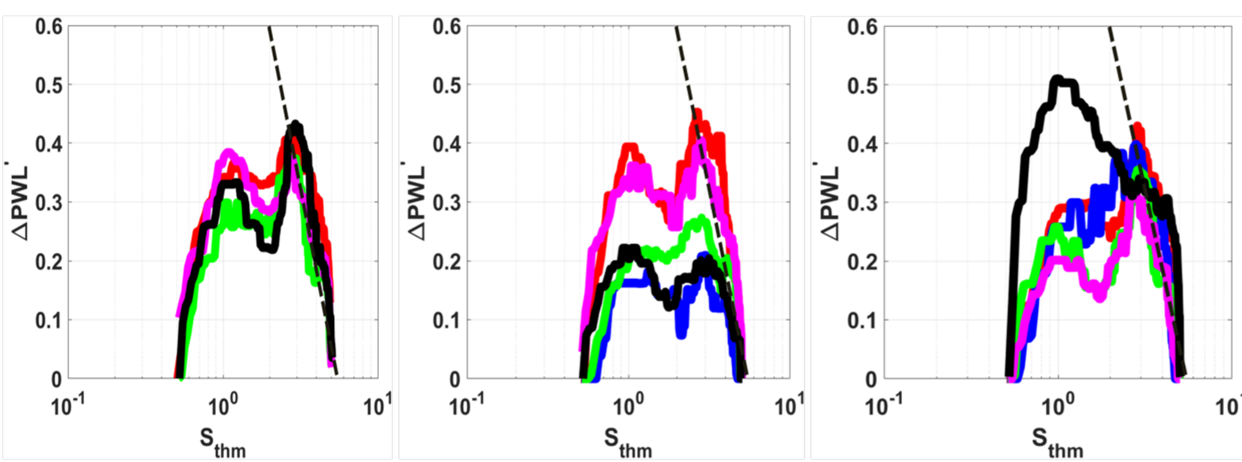

(a) (b) (c)

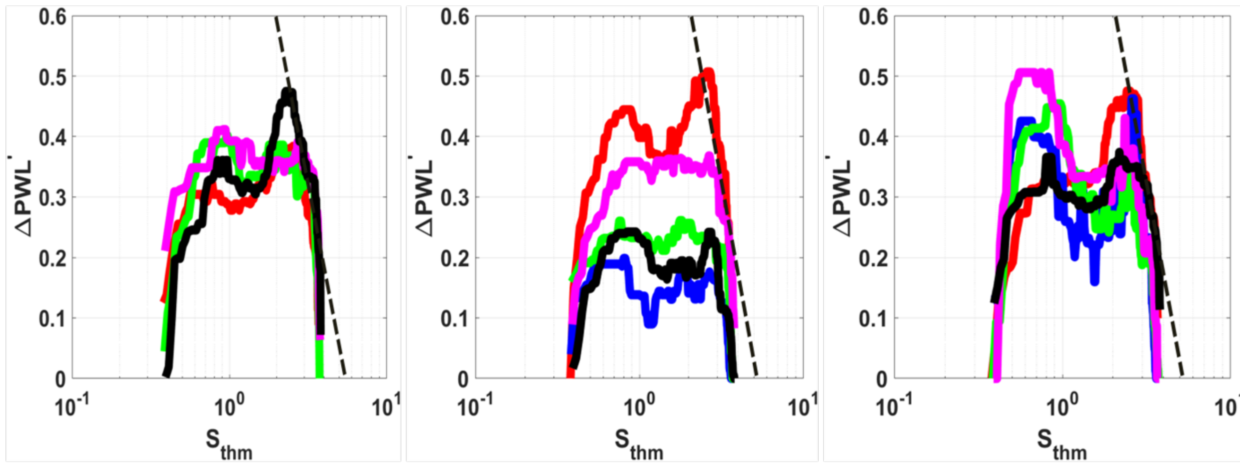

(d) (e) (f)

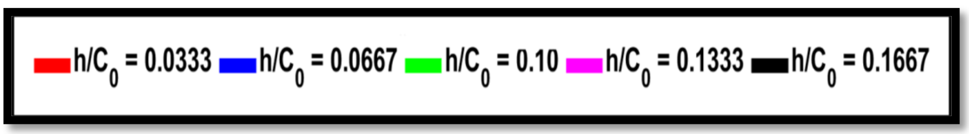

Fig.14. Variation of normalized sound power reduction $\Delta PWL'$ with modified Strouhal number S_{thm} at (a) $\lambda/C_0 = 0.033$ (b) $\lambda/C_0 = 0.066$ (c) $\lambda/C_0 = 0.2$ at $U = 30\ ms^{-1}$ and (d) $\lambda/C_0 = 0.033$ (e) $\lambda/C_0 = 0.066$ (f) $\lambda/C_0 = 0.2$ at $U = 40\ ms^{-1}$.

The present study reveals the presence of a geometric similarity condition at which the noise reduction is a function of four length scales, serration amplitude, gust wavelength λ_h i.e., U/f, serration wavelength (λ), and transverse integral length scale (Λ_t). Here we show that this finding is consistent with the assumption that the length l' ($\omega, h, \lambda, \Lambda_t$) of the acoustic sources along the sinusoidal trailing edge scales linearly with the modified Strouhal number. In the present analysis, the length l' of the acoustic source along the sinusoidal trailing edge can be expressed as

$$l'(\omega,h,\lambda, \Lambda_t) = \tilde{\eta}(h, \lambda, \Lambda_t)\, \lambda_h(\omega) = \eta(h)(1 + \log(\lambda/\Lambda_t)\, \lambda_h(\omega) \quad (18)$$

where $\tilde{\eta}\ (h, \lambda, \Lambda_t) = \eta(h)(1+\log(\lambda/\Lambda_t))$, $\tilde{\eta}$ and η are dimensionless constants. The total acoustic radiation from the sinusoidal trailing edge serration w_{sste} can be written as the acoustic power per tip w_{tip} multiplied by the number of tips N_{tip}, i.e., $w_{sste}(\omega) = w_{tip}(\omega)N_{tip}(\lambda)$ by assuming that the sound power radiated from each tip is roughly the same. Further, the acoustic power radiated from each tip is assumed to be equal to the length, l' of the source along the sinusoidal trailing edge and acoustic power per unit length is $w_l(\omega)$, then the acoustic power from the tip $w_{tip}(\omega)$ can be written as

$$w_{tip}(\omega) = w_l(\omega)l'(\omega, h, \lambda, \Lambda_t) \quad (19)$$

where l' is the length of the source given by Eq. (18)

The sound power radiation from the sinusoidal trailing edge serration can therefore be written as:

$$w_{sste}(\omega) = w_l(\omega)\,\tilde{\eta}(h, \lambda, \Lambda_t)\,\lambda_h(\omega) N_{tip}(\lambda) \qquad (20)$$

$$w_{sste}(\omega) = w_l(\omega)\eta(h)(1 + \log(\lambda/\Lambda_t))\,\lambda_h(\omega)\, N_{tip}(\lambda) \qquad (21)$$

where $\lambda_h = U/f$ and $N_{tip}(\lambda) = L/\lambda$, where L is the span of the airfoil.

The acoustic power from the baseline airfoil with a straight trailing edge can be written as,

$$w_{bl}(\omega) = w_l(\omega)L = w_l(\omega)N_{tip}(\lambda)\,\lambda \qquad (22)$$

The ratio of the acoustic power radiated from the sinusoidal trailing edge serrated airfoil to the baseline is therefore

$$w_{sste}(\omega)/w_{bl}(\omega) = \tilde{\eta}(h, \lambda, \Lambda_t)\,\lambda_h/\lambda' \qquad (23)$$

$$w_{sste}(\omega)/w_{bl}(\omega) = \eta(h)(1 + \log(\lambda/\Lambda_t))\,\lambda_h/\lambda' \qquad (24)$$

where λ' is the serration wavelength corresponding to the maximum noise reduction. λ' can be expressed in terms of serration amplitude and serration inclination angle $\tan(\theta') = 4h/\lambda'$. The ratio of the sound power from the sinusoidal trailing edge serrated airfoil and the baseline maybe written as :

$$w_{sste}(\omega)/w_{bl}(\omega) = \eta(h)(1 + \log(\lambda/\Lambda_t)\,\lambda_h \tan(\theta')/4h \qquad (25)$$

$$w_{sste}(\omega)/w_{bl}(\omega) = \eta(h)(1 + \log(\lambda/\Lambda_t)\,U \tan(\theta')/4fh \qquad (26)$$

$$w_{sste}(\omega)/w_{bl}(\omega) = \eta(h)(1 + \log(\lambda/\Lambda_t)\tan(\theta')/4fh/U \qquad (27)$$

$$w_{sste}(\omega)/w_{bl}(\omega) = \eta(h)(1 + \log(\lambda/\Lambda_t)\tan(\theta')/4s_{th} \qquad (28)$$

$$w_{sste}(\omega)/w_{bl}(\omega) \propto 1/S_{thm} \qquad (29)$$

where S_{thm} is the modified Strouhal number. The generalized equation for predicting the $\Delta PWL'$ is approximated as:

$$\Delta PWL' = a\log(S_{thm}) + b \qquad (30)$$

Table 3

Value of constants a and b for the best line fitted for two different velocities $30\ ms^{-1}$ *and* $40\ ms^{-1}$ where 'a' and 'b' are constants whose values are given in table 3 and are shown in [Fig. 14].

Velocity (ms^{-1})	*a*	*b*
30	-1.965	1.834
40	-0.524	0.786

7. Directivity characteristics

7.1. Sound power level directivity comparison of baseline and sinusoidal TE serrated NACA-65 airfoils for different serration parameters

The sound power level directivities of baseline and sinusoidal TE serrated NACA airfoils at λ/C_0 value of *0.2* are compared in [Fig. 15] for different h/C_0 values and jet velocities. The sound power levels are determined by integrating the power spectral densities over the range of frequencies from *4-10 kHz* at which the sinusoidal TE serrations provide significant noise reductions. In general, it is observed that baseline airfoil shows higher directivity as compared to the sinusoidal TE serrated airfoils formed for different h/C_0 values at fixed λ/C_0 value, even though they show a common feature of downstream directivity. It reveals that the acoustic radiations of both the baseline and TE serrated airfoils increase with the increase in jet velocities and lower radiations are observed for TE serrated airfoils at all emission angles. For both the baseline and TE serrated airfoils, the highest directivity is seen at an emission angle of 127.5^o.

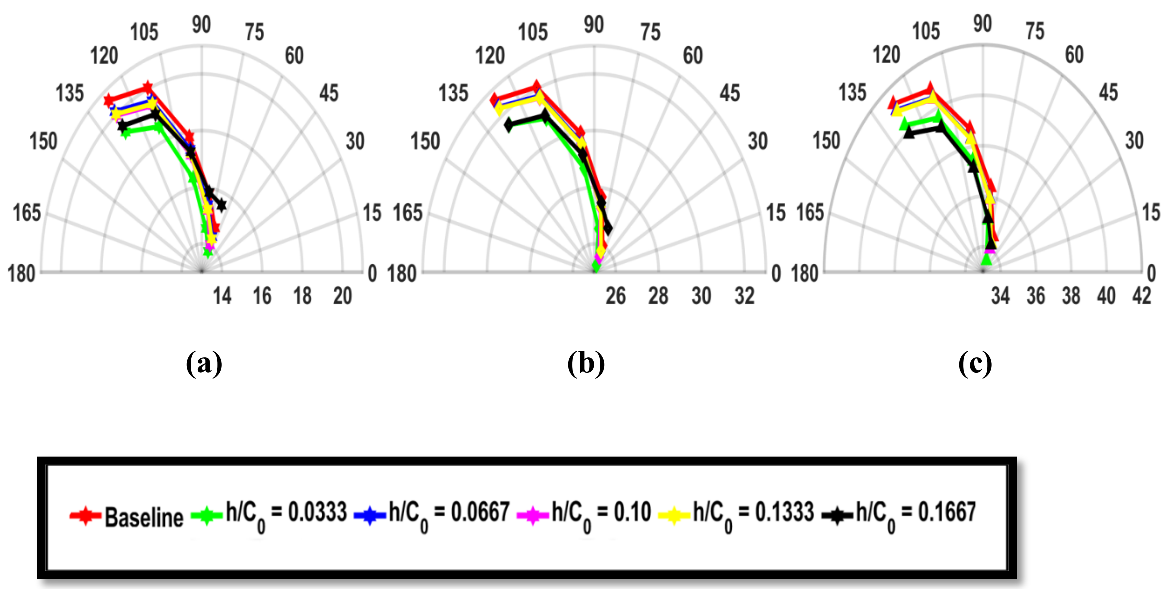

Fig.15. Sound power level directivity comparison of baseline and TE serrated airfoils ($\lambda/C_0 = 0.2$ for different h/C_0 values) at jet velocities of (a) $20\ ms^{-1}$ (b) $30\ ms^{-1}$ and (c) 40 ms^{-1}

The lower far-field acoustic radiations provided by the sinusoidal TE serrated airfoils may be due to the reduced surface pressure fluctuations close to the trailing edge as a result of the reduced velocity fluctuations as reported by Tang et al. [31]. In TE serrated airfoils, the surface pressure fluctuations close to the trailing edge are expected to be concentrated at the tip while in baseline straight edge airfoil the surface pressure fluctuations are concentrated throughout the span of the airfoil. In TE serrated airfoils tip sources are mainly radiating to the far-field and hence far-field noise is much lower than baseline airfoil, where the radiations occur throughout the span of the baseline. Also, the root sources are not contributing to the far-field noise in sinusoidal TE serrated airfoils due to the smooth mixing of the upper and lower boundary layers at the root.

As observed earlier, the presence of TE serrations is found to reduce the overall noise. This indicates that interaction noise is also reduced along with the TE noise. To understand the reduction of the leading edge noise component, we have plotted the sound power level directivity [Fig. 16]of baseline and TE serrated airfoil ($\lambda/C_0 = 0.2$, $h/C_0 = 0.166$) for three different range of frequencies ($0.1\text{-}4\ kHz$, $4\text{-}10\ kHz$ and $0.1\text{-}10\ kHz$). These frequencies are chosen to classify the dominant noise zones, namely, LE dominant $0.1\text{-}4\ kHz$ and TE dominant ($4\text{-}10\ kHz$) on the overall noise ($0.1\text{-}10\ kHz$). It is observed that from $0.1\text{-}4\ kHz$ [Fig. 16a]. both baseline and TE serrated airfoils show strong upstream directivity. In contrast, at frequencies from $4\text{-}10\ kHz$ [Fig. 16b], a strong downstream directivity is observed. However, for the overall range of $0.1\text{-}10\ kHz$, a strong upstream directivity is noticed in [Fig. 16c], similar to LE dominant range. Further, the radiation levels for all emission angles increase with the increase in jet velocities for all the above-mentioned cases.

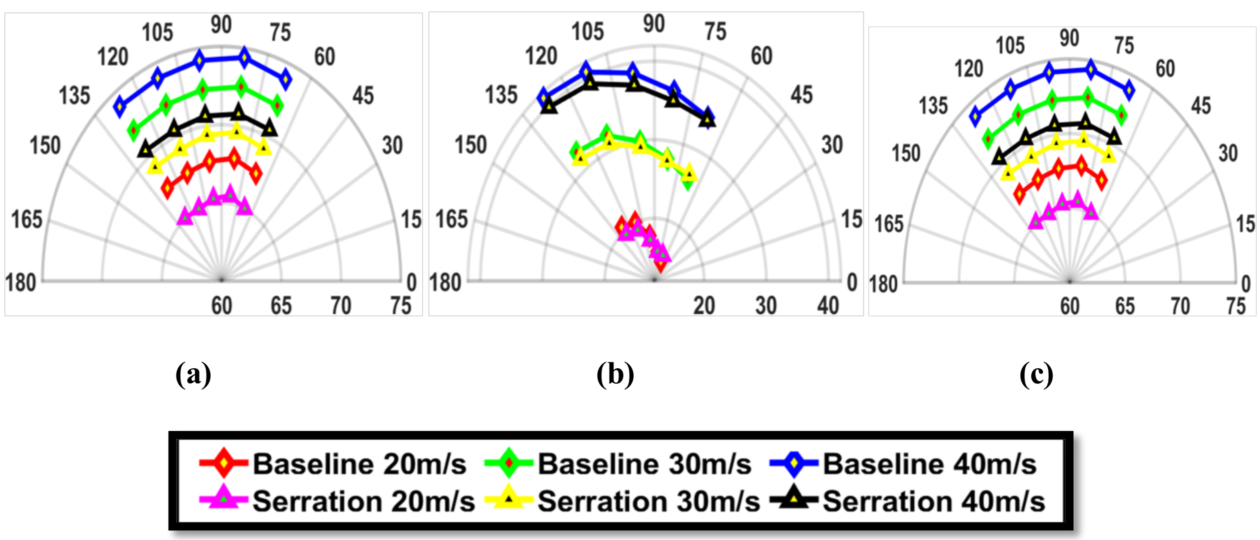

Fig.16. Sound power level directivity comparison of baseline and TE serrated airfoil ($\lambda/C_0 = 0.2$, $h/C_0 = 0.166$) obtained for the range of frequencies (a) $0.1\text{-}4\ kHz$ (b) $4\text{-}10\ kHz$ (c) $0.1\text{-}10\ kHz$ at $20\ ms^{-1}$, $30\ ms^{-1}$and $40\ ms^{-1}$ jet velocities.

Also, it is observed that the baseline radiates higher acoustic emission levels for all emission angles as compared to the TE serrated ones for all the range of frequencies mentioned above. For the range of frequencies *0.1-10 kHz* [Fig. 16c] and *0.1- 4 kHz* [Fig. 16a]; the highest directivity is observed at an emission angle of 67.5° for both the baseline and TE serrated plates at all jet velocities. Thus, it reveals that the frequencies lying in the range from *0.1- 4 kHz* lead to the shift in directivity from upstream to downstream. To understand the shift in directivity from upstream to downstream, the sound power level directivity of baseline and TE serrated airfoil (λ/C_0 = *0.166*, h/C_0 = *0.166*) at frequencies of *500 Hz*, *800 Hz*, and *1 kHz* are compared in [Fig. 17]. A striking feature observed is that the acoustic radiations occurring at a frequency of *500 Hz* [Fig. 17a] show upstream directivity for both the baseline and TE serrated airfoil and the highest directivity is observed at an emission angle of *67.5°*. At a frequency of *800 Hz* [Fig. 17b], the directivity of both the airfoils gradually shifts from upstream to the vertical direction (i.e., *90°* to the jet axis) and the highest directivity is observed at an emission angle of *90°*. At a frequency of *1 kHz* [Fig. 17c], both the airfoils show downstream directivity at all jet velocities, and the highest directivity is observed at an emission angle of *127.5°* similar to the range of the frequencies from *4-10 kHz* .

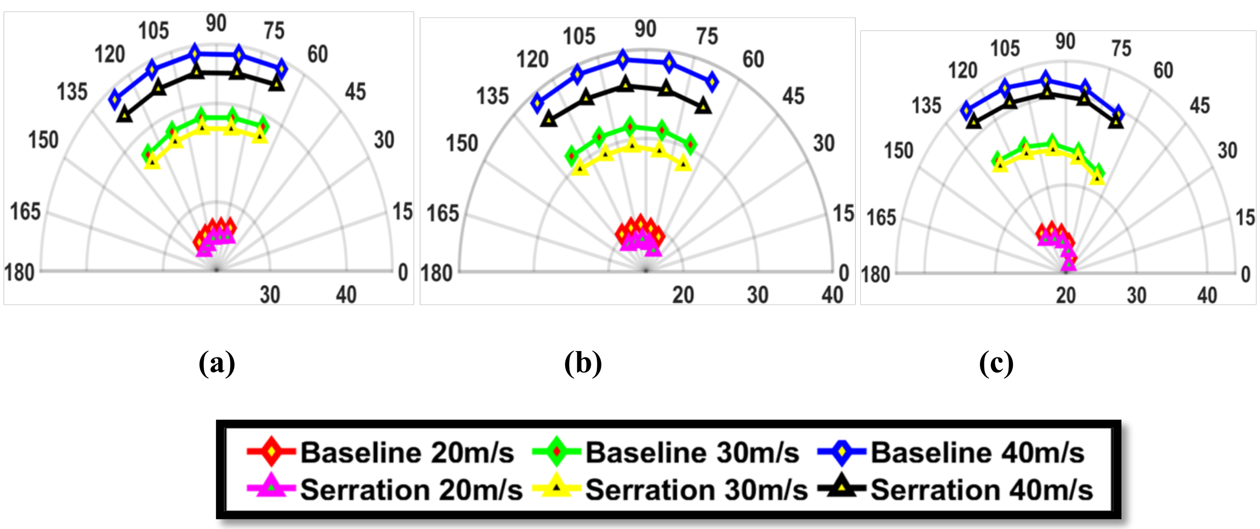

Fig.17. Sound power level directivity comparison of baseline and TE serrated airfoil (λ/C_0 = *0.166* h/C_0 = *0.166*) at frequencies of (a) *500 Hz* (b) *800 Hz* and (c) *1 kHz*.

For all the frequencies, *500 Hz*, *800 Hz*, and *1 kHz*, the baseline plate shows higher acoustic emission levels for all emission angles and the far-field acoustic radiations increase with the increase in jet velocities. The directivity shift observed above leads to a conclusion that there must be some feedback loop from the serrated TE which results in the reduction of the LE noise along with the TE noise and hence the overall noise. The feedback mechanism as mentioned above is evident from the switching of the directivity from downstream to upstream or vice versa. The potential mechanisms of the reduction of the interaction noise (low to mid frequencies i.e., *0.5 to about 4 kHz*,) might be due to the destructive interference between the upstream radiating acoustic waves from the TE and the radiations from the straight LE., while the reductions of self-noise (mid to high frequencies i.e.,*4 to about 10 kHz*) arises due to the redistribution of the radiated far-field acoustic emissions from the tip of the TE serrations; as reported by Ayton [32]. Thus, it reveals that the introduction of sinusoidal serrations acts as the best passive means for the reduction of total noise over a wide range of frequencies.

8. Velocity profiles

8.1. Mean boundary layer velocity profiles of baseline and TE serrated NACA-65 airfoils

In this section, the mean boundary layer velocity profiles for the baseline and sinusoidal TE serrated airfoils are compared to understand the modifications in the boundary layer due to the TE serrations. Hot-wire measurements were performed to measure the mean velocity profiles in the vicinity of the sinusoidal trailing edge.[Fig. 18a] shows the schematic of different sections of the sinusoidal profile at which measurements were taken.[Fig. 18b]shows the comparison between mean velocity profiles at the tip, root, and the hill of the sinusoidal serrations with the baseline. The data is acquired with the hot-wire sensor $10\,mm$ upstream of the trailing edge at a free stream velocity of $20\,ms^{-1}$. It is observed that the boundary layer is thicker at the root and thinner at the tip of the serrated airfoil. Further, the boundary layer at the hill is much thicker than the tip and the thickness is close to the root thickness. The boundary layer thickness of the baseline airfoil is in between the tip and root of the serrated airfoil. Earlier studies by Blake [33] and Stalnov et al. [34] reported that the surface pressure in the vicinity of the trailing edge and hence the far-field noise can be determined by integrating the product of the mean shear rate and the mean square velocity through the boundary layer. Blake [33] showed that the presence of a reduced mean velocity gradient results in the reduction of the surface pressure and hence the far-field noise. The presence of the thinner boundary layer at the tip of the serrated airfoil results in higher mean shear gradients and the thicker boundary layer at the root results in a lower mean velocity gradient, while the mean shear rate at the hill is close to the root. The boundary layer thickness of the baseline airfoil is in between the tip and root of the serrated airfoil. The presence of higher mean shear gradients at the tip of the serrated airfoil leads to a large surface pressure spectrum at the tip and hence the far-field noise from the tip of the serrated airfoil is higher as compared to root and oblique surface.

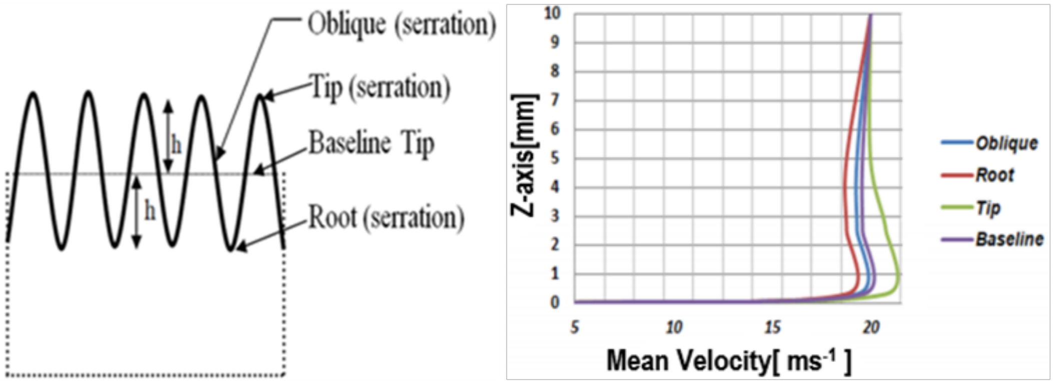

(a) **(b)**

Fig.18. (a) Schematic of the boundary layer profiles measured at different locations of the TE serrated NACA airfoil (b) Comparison of the boundary layer mean velocity profile of baseline, Root, Oblique/hill, and Tip of the TE serration for λ/C_0 = *0.2* and h/C_0 =*0.1667* at *0*◦ angles of attack.

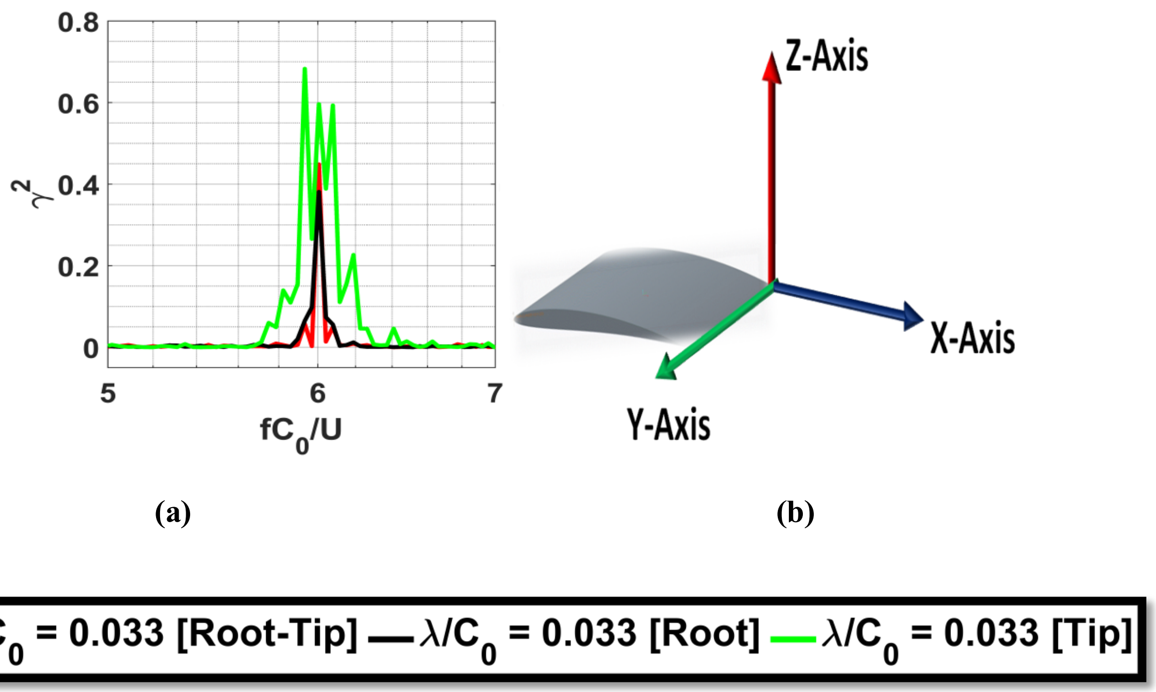

Fig.19. (a)The magnitude squared coherence comparison of Root -Tip, Root- Root & Tip- Tip for serration having λ/C_0 = *0.033* and h/C_0 =0.1667 at near wake zone for 20ms^{-1}at 0◦ angles of attack. (b) The coordinate axis of the aerofoil where,+X represents the streamwise direction; +Y represents the direction towards the spanwise direction of the foil, and +Z represents the normal to the chord and towards the phased microphone array.

The mean square spanwise coherence is compared between Tip –Tip, Tip-Root, and Root-Root of the TE serrations along spanwise [Fig. 19b] with Strouhal number in [Fig. 19a] to show that the surface pressure fluctuations are primarily concentrated at the tip of the TE serrations. It reveals that the presence of strong spanwise correlation at Tip-Tip of the serration indicates the presence of higher surface pressure fluctuations and hence the far-field noise as compared to the Root-Tip and Root-Root of the serration. Also, spanwise de-correlation observed at the Tip-Root and Root-Root of the TE serration indicates less noise radiations to the far-field as reported by Kim et. al. [35] for the LE serrations. Thus, it reveals that the significant noise radiations occur primarily from the tip of the TE serrated airfoil. The higher noise radiations provided by the baseline are due to the presence of noise radiations throughout the span of the airfoil, even though the mean shear rate is lower as compared to the tip of the serrated airfoil.

9. Conclusions

The present paper shows the effectiveness of the sinusoidal trailing edge serrations as a passive means for the reduction of airfoil broadband noise. A detailed systematic parametric study is performed to investigate the effect of serration amplitudes and wavelengths on the noise reduction performance of the serrated airfoil and hence to find out the best serration parameters which provide large noise reduction over a broad range of frequencies. Initially, the acoustic spectra of the baseline and the sinusoidal serrated airfoils are analytically predicted using the Weiner-Hopf method, by replacing the Chase model with the TNO model, since the TNO model considers the secondary leading edge interaction effects and provides better predictions of the surface pressure close to the trailing edge and hence the far-field noise. Further, the acoustic spectra and noise reductions obtained from the predictions are compared with the measured data, which showed good agreement over a broad range of frequencies. The comparison of acoustic spectra between the sinusoidal trailing edge serrations and V-shaped serrations for the same parametric conditions reveals that the sinusoidal serrations could emit lower far-field emissions and provide higher noise reductions over an abroad range of frequencies. It is also observed that the longer sinusoidal serrations provide higher noise reductions as compared to shorter ones, while both the narrow and wider serrations show significant noise reductions. Also, the trailing edge serrations are observed to reduce the turbulence interaction noise along with airfoil self-noise, thus reducing the overall far-field noise. The reason for the reductions of overall noise (i.e., interaction + self-noise) could be due to the smooth mixing of the boundary layers from the suction and pressure surfaces, at the root of the serrations while at the tip of the serrations the mixing of the boundary layers is not possible, similar to the baseline case, where the mixing of the boundary layers is not possible throughout the span. The contribution to far-field noise arises from the surface pressure fluctuations concentrated at the tip of the TE serrations whereas noise emissions occur from the entire span of the baseline airfoil, which results in the reductions of the overall far-field noise due to TE serrations. The tip source is the dominant noise source in TE serrations while the root source and oblique surface are not dominant. The reductions of the overall far-field noise due to

TE serrations could be due to the destructive interference of the acoustic radiations from the subsequent tip of the serrations as well as the incoherent radiations from the root/oblique sources. The inverse variation of the sound power radiated from the sinusoidal serrated trailing edge with the modified Strouhal number indicates that the length of the sources along the sinusoidal trailing edge varies linearly with the gust wavelength. The radiations in TE serrated airfoils primarily arise from the tips of the serration, which is evident from the formation of a thinner boundary layer as compared to the root as well as hill. Also, the radiations from the neighboring tip sources interfere incoherently and reduce the airfoil self-noise. The weak acoustic radiations (upstream propagating) from the tips of the TE serrations could interfere destructively with the radiations from the LE and reduces the interaction noise along with the self-noise, which is evident from the shift in the directivity from downstream to upstream. Thus, it indicates that the reduction of overall noise might be due to the formation of a feedback loop between the acoustic waves originated from the tip of the serrations and the straight leading edge.

Data Availability:

Some or all data, models, or codes that support the findings of this study are available from the corresponding author upon reasonable request.

Acknowledgment:

The authors gratefully acknowledge that the current work has been supported by DST (SERB, (ECR/2016/000640)

References:

[1] R.K. Amiet, Effect of the incident surface pressure field on noise due to turbulent flow past a trailing edge, J. Sound Vib. 57 (1978) 305–306. https://doi.org/10.1016/0022-460X(78)90588-6.

[2] R.K. Amiet, Acoustic radiation from an airfoil in a turbulent stream, J. Sound Vib. 41 (1975) 407–420. https://doi.org/10.1016/S0022-460X(75)80105-2.

[3] R.K. Amiet, Noise due to turbulent flow past a trailing edge, J. Sound Vib. 47 (1976) 387–393. https://doi.org/10.1016/0022-460X(76)90948-2.

[4] M. Azarpeyvand, M. Gruber, P.F. Joseph, An analytical investigation of trailing edge noise reduction using novel serrations, in: 19th AIAA/CEAS Aeroacoustics Conf., 2013: p. 8. https://doi.org/10.2514/6.2013-2009.

[5] T. Bachmann, S. Klän, W. Baumgartner, M. Klaas, W. Schröder, H. Wagner, Morphometric characterisation of wing feathers of the barn owl Tyto alba pratincola and the pigeon Columba livia, Front. Zool. 4 (2007) 1–15. https://doi.org/10.1186/1742-9994-4-23.

[6] T.F. Brooks, D.S. Pope, M.A. Marcolini, Airfoil self-noise and prediction, NASA Ref. Publ. (1989).

[7] M. Gruber, Airfoil noise reduction by edge treatments by Mathieu Gruber Thesis for the

degree of Doctor of Philosophy, Inst. Sound Vib. Res. PhD (2012).

[8] T. Dassen, R. Parchen, J. Bruggeman, F. Hagg, Results of a wind tunnel study on the reduction of airfoil self-noise by the application of serrated blade trailing edges, in: Proceeding Eur. Union Wind Energy Conf. Exhib., 1996: pp. 800–803. https://reports.nlr.nl/xmlui/handle/10921/1359 (accessed March 27, 2021).

[9] S. Oerlemans, P. Sijtsma, B. Méndez López, Location and quantification of noise sources on a wind turbine, J. Sound Vib. 299 (2007) 869–883. https://doi.org/10.1016/j.jsv.2006.07.032.

[10] D.J. Moreau, C.J. Doolan, Noise-reduction mechanism of a flat-plate serrated trailing edge, in: AIAA J., 2013: pp. 2513–2522. https://doi.org/10.2514/1.J052436.

[11] T. Dassen, R. Parchen, G. Guidati, S. Wagner, S. Kang, A.E. Khodak, Comparison of measured and predicted airfoil self-noise with application to wind turbine noise reduction, Eur. Wind Energy Conf. Exhib. (1997).

[12] A. Sivakumar, R. Porteous, A. Mimani, C.J. Doolan, An experimental investigation of turbulent boundary-layer interaction with different serrated trailing-edge configurations, in: Acoust. 2015 Hunt. Val., 2015. https://dspace.nal.gov.au/xmlui/handle/123456789/363 (accessed March 27, 2021).

[13] C.J. Doolan, D.J. Moreau, A Review of Airfoil Trailing Edge Noise with Some Implications for Wind Turbines, Int. J. Aeroacoustics. 14 (2015) 811–832. https://doi.org/10.1260/1475-472x.14.5-6.811.

[14] T.P. Chong, P.F. Joseph, M. Gruber, Airfoil self noise reduction by non-flat plate type trailing edge serrations, Appl. Acoust. 74 (2013) 607–613. https://doi.org/10.1016/j.apacoust.2012.11.003.

[15] M. Herr, W. Dobrzynski, Experimental investigations in low noise trailing edge design, in: Collect. Tech. Pap. - 10th AIAA/CEAS Aeroacoustics Conf., 2004: pp. 54–67. https://doi.org/10.2514/6.2004-2804.

[16] P. Zhou, S. Zhong, X. Zhang, On the effect of velvet structures on trailing edge noise: experimental investigation and theoretical analysis, J. Fluid Mech. 919 (2021). https://doi.org/10.1017/jfm.2021.374.

[17] R.D. Sandberg, L.E. Jones, Direct numerical simulations of low Reynolds number flow over airfoils with trailing-edge serrations, J. Sound Vib. 330 (2011) 3818–3831. https://doi.org/10.1016/j.jsv.2011.02.005.

[18] F. Avallone, S. Pröbsting, D. Ragni, Three-dimensional flow field over a trailing-edge serration and implications on broadband noise, Phys. Fluids. 28 (2016). https://doi.org/10.1063/1.4966633.

[19] C. Arce León, D. Ragni, S. Pröbsting, F. Scarano, J. Madsen, Flow topology and acoustic emissions of trailing edge serrations at incidence, Exp. Fluids. 57 (2016) 1–17. https://doi.org/10.1007/s00348-016-2181-1.

[20] S. Narayanan, P. Chaitanya, S. Haeri, P. Joseph, J.W. Kim, C. Polacsek, Airfoil noise reductions through leading-edge serrations, Phys. Fluids. 27 (2015). https://doi.org/10.1063/1.4907798.

[21] S.K. Sushil, M. Garg, S. Narayanan, Estimation of the lower cut-off frequency of an anechoic chamber: An empirical approach, Int. J. Aeroacoustics. 19 (2020) 57–72. https://doi.org/10.1177/1475472X20905070.

[22] R.K. Amiet, Acoustic radiation from an airfoil in a turbulent stream, J. Sound Vib. 41 (1975) 407–420. https://doi.org/10.1016/S0022-460X(75)80105-2.

[23] M. Roger, S. Moreau, Extensions and limitations of analytical airfoil broadband noise

models To cite this version : HAL Id : Hal-00566057 airfoil broadband noise models, (2012).

[24] P. Chaitanya, P. Joseph, S. Narayanan, C. Vanderwel, J. Turner, J.W. Kim, B. Ganapathisubramani, Performance and mechanism of sinusoidal leading-edge serrations for the reduction of turbulence-aerofoil interaction noise, J. Fluid Mech. 818 (2017) 435–464. https://doi.org/10.1017/jfm.2017.141.

[25] B. Lyu, L.J. Ayton, Rapid noise prediction models for serrated leading and trailing edges, J. Sound Vib. 469 (2020) 115136. https://doi.org/10.1016/j.jsv.2019.115136.

[26] D.M. Chase, The character of the turbulent wall pressure spectrum at subconvective wavenumbers and a suggested comprehensive model, J. Sound Vib. 112 (1987) 125–147. https://doi.org/10.1016/S0022-460X(87)80098-6.

[27] O. Stalnov, P. Chaitanya, P.F. Joseph, Towards a non-empirical trailing edge noise prediction model, J. Sound Vib. 372 (2016) 50–68. https://doi.org/10.1016/j.jsv.2015.10.011.

[28] M. Roger, S. Moreau, Back-scattering correction and further extensions of Amiet's trailing-edge noise model. Part 1: Theory, J. Sound Vib. 286 (2005) 477–506. https://doi.org/10.1016/j.jsv.2004.10.054.

[29] S. Moreau, M. Roger, Back-scattering correction and further extensions of Amiet's trailing-edge noise model. Part II: Application, J. Sound Vib. 323 (2009) 397–425. https://doi.org/10.1016/j.jsv.2008.11.051.

[30] M. Sanjosé, S. Moreau, B. Lyu, L. Ayton, Analytical, numerical and experimental investigation of trailing-edge noise reduction on a controlled diffusion airfoil with serrations, 25th AIAA/CEAS Aeroacoustics Conf. 2019. (2019). https://doi.org/10.2514/6.2019-2450.

[31] H. Tang, Y. Lei, Y. Fu, Noise reduction mechanisms of an airfoil with trailing edge serrations at low mach number, Appl. Sci. 9 (2019). https://doi.org/10.3390/app9183784.

[32] L.J. Ayton, Analytic solution for aerodynamic noise generated by plates with spanwise-varying trailing edges, J. Fluid Mech. 849 (2018) 448–466. https://doi.org/10.1017/jfm.2018.431.

[33] W.K. Blake, Turbulent boundary-layer wall-pressure fluctuations on smooth and rough walls, J. Fluid Mech. 44 (1970) 637–660. https://doi.org/10.1017/S0022112070002069.

[34] O. Stalnov, P. Chaitanya, P.F. Joseph, Prediction of broadband trailing-edge noise based on Blake model and Amiet theory, 21st AIAA/CEAS Aeroacoustics Conf. (2016) 1–19. https://doi.org/10.2514/6.2015-2526.

[35] J. Kim, P. Moin, R. Moser, Turbulence statistics in fully developed channel flow at low reynolds number, J. Fluid Mech. 177 (1987) 133–166. https://doi.org/10.1017/S0022112087000892.